Porous silica microscaffolds for nanoparticle immobilization

Patrícia Pereira da Silva

Thesis to obtain the Master of Science Degree in

Chemical Engineering

Supervisor: Prof. Dr. Ana Clara Lopes Marques

Examination Committee

Chairperson: Prof. Dr. Mário Berberan

Supervisor: Prof. Dr. Ana Clara Lopes Marques

Member of Committee: Prof. Dr. Maria Clara Gonçalves

December 2020

Acknowledgments

Through this peculiar year with several challenges, this work would not be done without all the encouragement, support, and understanding that have been given to me.

I would like to express my gratitude and appreciation to Mário Vale for all help and advice and to Prof. Dr. Ana C. Marques, who supported me, led me, and offered me the opportunity to carry out this work.

Lastly, an enormous thank you to the friends who, with their words, gave me the motivation I needed and last but not least, to my parents, to whom I dedicate this work since a simple thank you is not even enough to thank all the effort they have made so I could reach this point.

Abstract

The present work regards the enlightenment of porous silica microspheres formation and their suitability as microscaffolds for immobilization of nanoparticles with scope for photocatalysis applications. Such porous microspheres were prepared via sol-gel technique with a water-in-oil microemulsion as a template inducing phase separation through spinodal decomposition, which led to interconnected macroporosity. These materials have great potential since they can be loaded with different chemical species, depending on the application preferred. Besides, their hybrid feature due to tetraethoxysilane (TEOS) and (3-Glycidyloxypropyl)trimethoxysilane (GPTMS) as silica precursors, provide them multifunctionality.

With the aim to find a precise approach that permits the control of pore size, shape, and morphology of the microspheres, two main methods were performed: condensation stimulated by pH and by temperature. Within those, the influence of various parameters in the reaction were evaluated, such as the addition of ammonia according to temperature, the amount of the precursor solution, the amount of surfactant, the hydrolysate addition's rate to the emulsion, hydrolysis duration and the hydrolysate's viscosity.

The microspheres that exhibited the desired final properties were found for a 30-minute addition to the emulsion of a pre-hydrolysate with a viscosity of 9.20 cP, following a specific temperature profile during condensation.

After the immobilization process, the presence of Aeroxide® P25 commercial TiO_2 nanoparticles within the microspheres were confirmed by Fourier transformed infrared spectroscopy (FTIR) and scanning electron microscopy (SEM-EDS) proving the capability of these microscaffolds as supports.

Keywords: Porous microspheres, microscaffolds, sol-gel, macroporosity, silica

Resumo

O presente trabalho aborda a formação de microesferas porosas de sílica e a sua capacidade para imobilização de nanopartículas, com foco em aplicações de fotocatálise. Tais microesferas porosas foram preparadas por metodologia sol-gel em microemulsão (água-em-óleo) e com separação de fases por decomposição espinodal, o que levou à formação de macroporosidade interligada. Estes materiais apresentam grande potencial, pois permitem a impregnação/imobilização de diferentes espécies químicas, dependendo da aplicação pretendida. Além disso, o seu caráter híbrido, que provém dos precursores de sílica tetraetoxisilano (TEOS) e (3-glicidiloxipropil)trimetoxissilano (GPTMS), confere-lhes multifuncionalidade.

Com o objetivo de controlar a porosidade, a forma e a morfologia das microesferas, dois métodos foram aplicados: condensação estimulada pelo pH e pela temperatura. Dentro destes, foi avaliada a influência de diversos parâmetros na reação, como a adição de amónia de acordo com a temperatura, a quantidade de solução precursora, a quantidade de surfactante, a taxa de adição do hidrolisado à emulsão, o tempo de hidrólise e a viscosidade do hidrolisado.

As microesferas que exibiram as propriedades desejadas foram obtidas para uma adição de 30 minutos à emulsão de um pré-hidrolisado com viscosidade de 9.20 cP, seguindo um perfil específico de temperatura durante a condensação.

Após o processo de imobilização, a presença de nanopartículas comerciais Aeroxide® P25 (TiO$_2$) nas microesferas foi confirmada pela espetroscopia de infravermelho de Fourier (FTIR) e por microscopia eletrónica (SEM-EDS), comprovando a capacidade destas microesferas como suportes de nanopartículas.

Palavras-chave: Microesferas porosas, sol-gel, macroporosidade, sílica

Contents

List of Figures

List of Tables

Nomenclature/Abbreviations/Symbol list

GPTMS – (3-Glycidyloxypropyl) trimethoxysilane;

HBL – Hydrophilic-lipophilic balance;

HCl – Hydrochloric acid;

MCs – Microcapsules;

MSs – Microspheres;

NG – Nucleation-growth phase-separation:

NPs – Nanoparticles;

O/W – Oil-in-water emulsion;

O/W/O – Oil-in-water-in-oil emulsion;

SD – Spinodal decomposition phase-separation;

TiO_2 – Titanium dioxide;

TEOS – Tetraethoxysilane or tetraethyl orthosilicate;

TMOS – Tetramethoxysilane;

T_{room} – Room temperature;

W/O – Water-in-oil emulsion;

W/O/W – Water-in-oil-in-water emulsion.

1. Introduction

1.1. Motivation

In the last decades, microspheres have been intensely studied due to their appliance in several fields of interest related to sustainability and innovation. Depending on their structure and morphology, they may be suitable for catalysis, separation, chromatography, controlled release, storage and conversion of energy, and so on. Macroporosity enables the extent of the microspheres' functionality, particularly for their loading with selected active species allowing more effective and sustainable processes. Their production from components as TEOS and GPTMS provide them multifunctionality from inorganic and organic materials; thus, the loading can be entrapped physically and through chemical reactions.

The main principle of this work is to attempt reproducibility of a method to attain macroporous silica microspheres within the research scope developed in Technology Platform on Microencapsulation and Immobilization (http://web.tecnico.ulisboa.pt/ana.marques/SiteTPMI/). These microspheres as silica materials offer biocompatibility, biodegradability, chemical resistance, thermal stability and are non-toxic for the environment. As supports (microscaffolds), they provide the surface area necessary for high dispersion and immobilization of active components (metals, metal oxides, enzymes, or other species). They are prepared by sol-gel accompanied by microemulsion technology. Phase separation by spinodal decomposition determines their inner structure. Thus, finding a precise method that allows control of pore size, shape and morphology is an essential upturn to the production of tailored microspheres and that is only possible if their formation process is enlightened.

1.2. Objectives

This work is centred on the development of silica microspheres with interconnected macroporosity. The objectives are producing those by combining sol-gel technique with microemulsion technology contributing for a better understanding of their formation mechanism and achieving a reproducible procedure to that aim based on the already developed method of previous works [1–3].

As-prepared microspheres are characterized in order to study their morphology, microstructure, and composition to recognize their suitability as supports of TiO_2 nanoparticles, to further application in photocatalytic systems in wastewater purification.

The work strategy relied on the following:

- The synthesis' optimization was made by studying the effect of temperature, pH, viscosity, reaction's time, and concentration of reactants in the reaction medium through optical microscopy;
- Evaluation of the microstructure of the MSs by SEM-EDS, FTIR-ATR, and TGA;
- Nanoparticles immobilization into the microspheres macroporosity;
- Proposal of a new photocatalytic pilot reactor for testing of the successful developed macroporous microspheres.

1.3.   Structure

This dissertation is divided into six chapters having the following structure:

Chapter 1 – It includes the framework of the thesis, with the main objectives and its structure.

Chapter 2 – This chapter englobes the State of the Art, some definitions, and essential concepts.

Chapter 3 – Englobes the materials used and the experimental procedures for the developing MSs, their Characterization, and TiO_2 Immobilization.

Chapter 4 – Comprises the obtained results of the experiment and relative discussion.

Chapter 5 – A brief conclusion and future work perspectives are presented.

Chapter 6 – The last section includes a proposal for MSs testing as support in photocatalytic systems.

2. Overview

2.1. Initial Concepts

2.1.1. Sol-gel process

The sol-gel process, defined by IUPAC, is the formation of a network by reactions of precursor(s) through a *sol* – colloidal particles or polymers in suspension in a liquid – that by its gelation leads to the *gel* formation – solid colloidal, or porous polymer network that surrounds and supports a continuous fluidic phase [4]. After a thermic treatment of the gel, it is possible to produce the desired material with a determined morphology (powder, fibre, film, and monolith) [5]. Figure 1 demonstrates this formation in a simplified way.
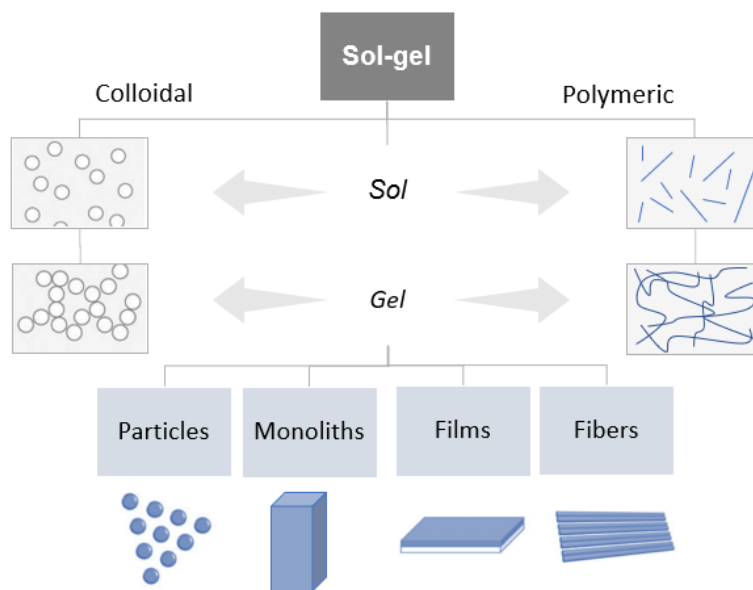
Figure 1 - Illustration of the process and exemplificative products of the sol-gel process. Adapted from [5]

The sol-gel approach is very well-known and widely used to synthesize silica-based materials from alkoxysilanes. It involves the following steps: hydrolysis, condensation, gelation, ageing, and drying.

Alkoxysilanes are the most used precursors due to their capability of reinforcement (particularly TMOS and TEOS). They have strong covalent Si–O bonds and are immiscible with water because of their alkyl groups' hydrophobic nature. Consequently, the hydrolysis and condensation reactions of these silanes have been studied in different circumstances. The sol-gel chemical reactions can be simply described by Equations 1–3 [6–9].

$$Hydrolysis: \quad (RO)_3Si-OR + H_2O \rightleftarrows (RO)_3Si-OH + ROH \tag{1}$$

$$Condensation: (RO)_3Si-OH + RO-Si(OR)_3 \rightleftarrows (RO)_3Si-O-Si(RO)_3 + ROH \tag{2}$$

$$Condensation: (RO)_3Si-OH + HO-Si(RO)_3 \rightleftarrows (RO)_3Si-O-Si(RO)_3 + H_2O \tag{3}$$
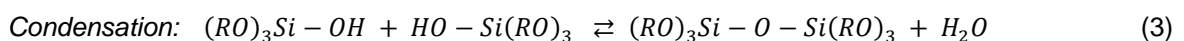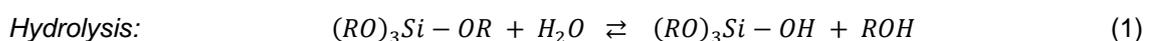
As it can be seen in Equations 1–3, the formation of Si-O-Si units – condensation – is dependent on the occurrence of hydrolysis, and it can happen by water or alcohol removal, depending on the reaction's extension, and therefore the Si/H_2O molar ratio. For example, increasing the water content, i.e., lowering Si/H_2O ratio, leads to the formation of silanol groups over Si-O-Si groups, which promotes condensation by Equation (3). Besides this reliance, these reactions are known to progress concomitantly since the beginning of the sol-gel reaction. Although depending on parameters such as pH (which affects relative hydrolysis to condensation rate – Figure 2), the type of solvent, and Si/H_2O molar ratio, it is possible to force hydrolysis' completion. Pre-hydrolysis is employed in some cases, aiming at a complete hydrolyzation of the precursors for an increased yield and better control of the network development through polymerization – "two-step" sol-gel reaction [7,10].
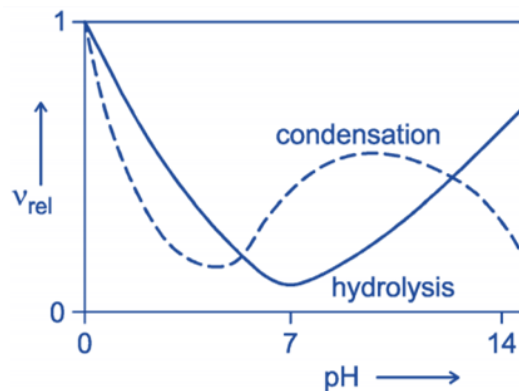
Figure 2 - Relative rates of hydrolysis and condensation reactions of alkoxysilanes accordingly to pH. Adapted from [7]

By analyzing Figure 2, hydrolysis has a minimum rate at pH 7 and increases tremendously, either with acidity or alkalinity. Instead, condensation has its minimum rate at pH 5 and maximum around 9-10, one of the points where it is faster than hydrolysis [7–9].

Other important parameters in a sol-gel reaction are the number and the volume of the alkoxy groups (may have inductive and steric effects on hydrolysis rate), type of catalyst, chemical additives, temperature, and pressure [7].

Hydrolysis

In alkoxysilanes-based systems, the hydrolysis of Si–OR groups generates Si-OH groups, essential for condensation reaction. Under acidic conditions, the oxygen atom of Si-OR group is protonated, creating a good leaving group (R-OH); under basic conditions, a nucleophilic attack happens where the OH⁻ attacks the silicon atom exchanging the alkoxide group (OR) for the hydrolytic species (OH) [7].

Since alkoxysilanes are hydrophobic, alcohols are used as solvents – alcohols of the same alkoxy group are preferred, so alcohol exchange reactions are prevented – to produce a homogeneous reaction mixture. Still, if a pre-hydrolysis is used, under stirring, the resultant alcohol inherent to it will eventually be enough to homogenate the solution. A catalyst may also be employed to accelerate the reaction [7–9]. Both reactions with acid and basic catalysts are shown in Figure 3 and Figure 4, respectively.
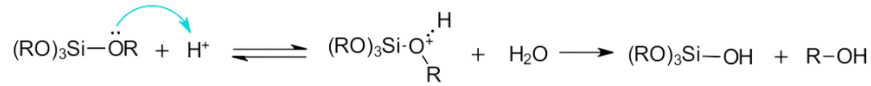
Figure 3 - Hydrolysis of alkoxysilanes under acidic conditions [7–9]
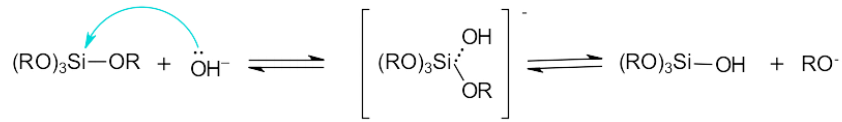
Figure 4 - Hydrolysis of alkoxysilanes under basic conditions [7–9]

Condensation

The condensation reactions involve the previous Si-OH groups (formed through hydrolysis) leading to the formation of oxide species. The course of this reaction is either by Equation 2 or 3 depending on the pH and Si/H_2O ratio [7,8].

Figure 5 and Figure 6 illustrate the differences between acidic and basic condensation reactions.
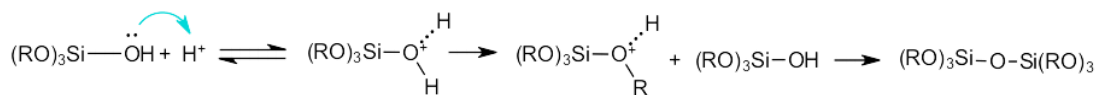
Figure 5 - Condensation of (RO)$_3$Si-OH under acidic conditions [7–9]
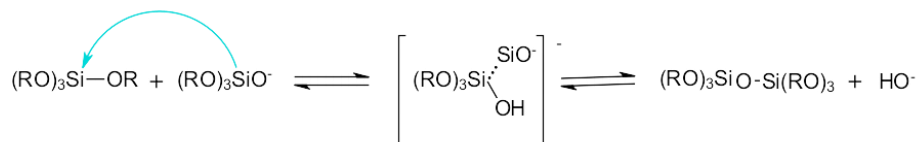
Figure 6 - Condensation of (RO)$_3$Si-OR under basic conditions [7–9]

Gelation, ageing, and drying

As the condensation reaction keeps going, the number of siloxane groups will increase and start linking with each other in the sol, leading to an incipient network formation. The resultant clusters aggregate to form the gel network – gelation [4,7–9]. This phenomenon depends highly on the pH level, and a significant increase in the viscosity of the solution is observed. Changes in the gel's chemical and physical structure happen, and the gel's properties also change. In drying, entrapped volatiles (water and alcohol) are outcasted, leading to network shrinking and strengthening: the wet gel is submitted to an adequate higher temperature or lower pressure to shrinking of the gel, then new Si-O-Si bridges are formed, which drives to stiffing of the network. After this point, the network is too stiff to suffer more shrinking meaning surface tension is no longer able to deform it. Instead, cracking of the structure is hugely probable since the tension in the gel is considerably high. To avoid this, a slow shrinking process and large pore network are preferred [4,7,9].

5

2.1.2. Emulsions

Emulsions are examples of colloidal systems with increased size in which there is one phase in the form of droplets dispersed into a continuous phase, and they can be introduced as the following [11–15]:

- Water-in-oil (W/O) emulsion – water droplets dispersed in an oil phase (Figure 7 (i));
- Oil-in-water (O/W) emulsion – oil droplets dispersed in water (Figure 7 (ii));
- Water-in-Oil-in-Water (W/O/W) emulsion – dispersed (in water) oil globules which contain smaller aqueous droplets (Figure 7 (iii));
- Oil-in-Water-in-Oil (O/W/O) emulsion – dispersed (in oil) water globules that contain smaller oil droplets (Figure 7 (iv)).
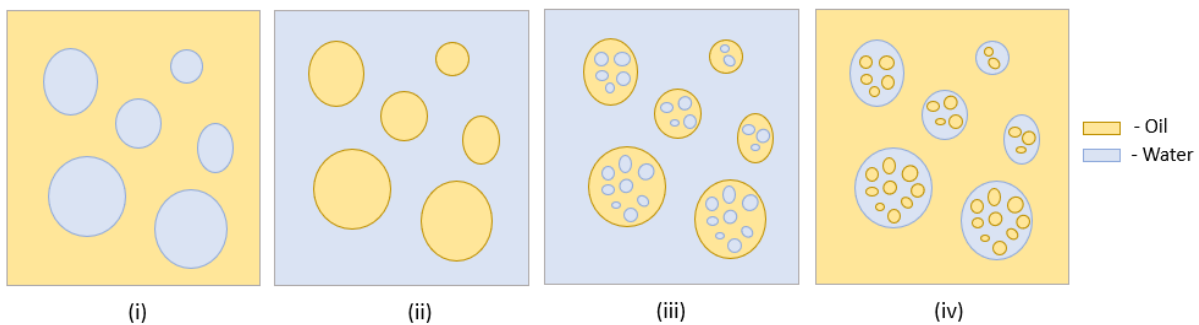
Figure 7 - Illustrative representation of the different forms of emulsions. Simple emulsions: (i) W/O, (ii) O/W. Double emulsions: (iii) W/O/W, (iv) O/W/O. Adapted from [11,12]

Emulsions are metastable systems (kinetically stable but thermodynamically unstable), so to avoid phase aggregation, repulsion forces are needed between the droplets, and for that purpose, a surfactant and energy input are required. It enables a stabilization of the emulsion by decreasing the superficial tension and droplet's coalescence. The surfactants or emulsifiers are stabilizer molecules, with an amphiphilic structure, i.e., containing a hydrophilic group, polar or ionic head groups, and a hydrophobic tail soluble in the organic phase, typically a hydrocarbon chain. Thus, they act as intermediates between the aqueous and organic phases – Figure 8 [11,14,16].

The most compacted droplet arrangement of preserved spherical droplets is for a droplet volume fraction – the ratio between droplets and continuous phase volume – of 74%. Emulsions that exceed this value are called HIPE (high internal phase emulsion) emulsions, and their structure is either composed by deformed or polydisperse droplets [7,13].

The surfactant's choice lies in the type of intended emulsion and where it will be engaged in the interface. Several empirical approaches predict its positioning, and HLB (hydrophile–lipophile balance) value is the most used. It gives the affinity between hydrophilic and hydrophobic groups, i.e., the affinity for water and oil. The values of this parameter go from 0 to 60. Values greater than 10 suggest an affinity for water (hydrophilic), while values lower than 10 indicate an affinity for oil (lipophilic) [10,11,16].
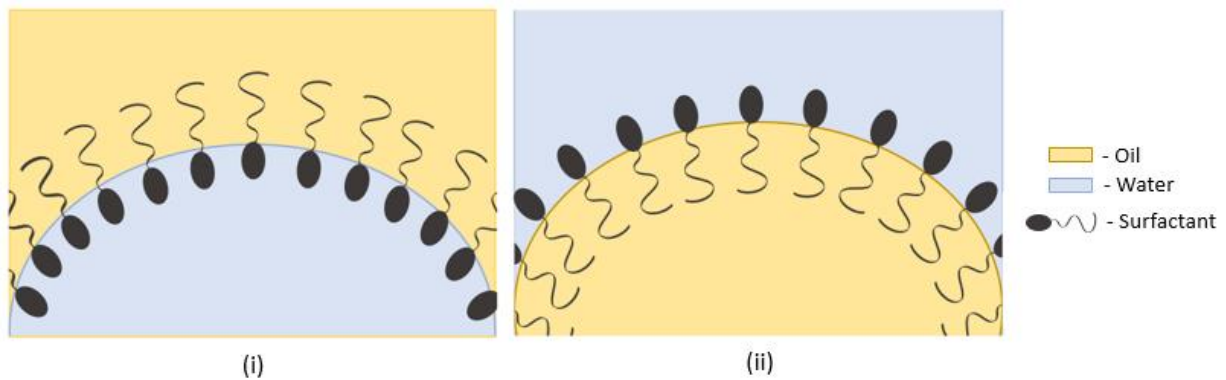
Figure 8 - Illustrative representation of the surfactant distribution at water/oil interface for (i) W/O emulsion and (O/W) emulsion. Adapted from [11–13]

2.1.3. Phase-separation

After all the efforts for understanding phase-separation occurrence, it can be an undesirable spontaneous phenomenon in the production of materials in which a uniform distribution of the functional groups within a matrix is required or an enforced pathway for the preparation of porous scaffolds [17–19].

Phase-separation is the creation of a new phase in a homogeneous system, forming heterogeneity. Depending on where the phase boundary is traversed in the phase diagram, this dynamic can occur by the following mechanisms: nucleation-growth or spinodal decomposition [14,20].

Nucleation-growth is a common phase separation mechanism and is often associated with crystallization from solution. Spinodal decomposition is less frequent and has been utilized to produce well-defined heterogeneous architectures.

- Nucleation-growth – takes place between binodal and spinodal lines (point N, Figure 9) wherein undergoes a metastable equilibrium, and it can occur by [14,21,22]:
    1. thermally induced microscopic composition fluctuation – homogeneous nucleation;
    2. impurity or inclusions which offer higher energy sites favourable for the nucleation – heterogeneous nucleation.
- Spinodal decomposition – takes place within the spinodal line (point M, Figure 9) wherein undergoes an unstable equilibrium, and it can occur when infinitesimal composition flocculation happens and destabilize the system, bringing it to a local or global energetic minimum.
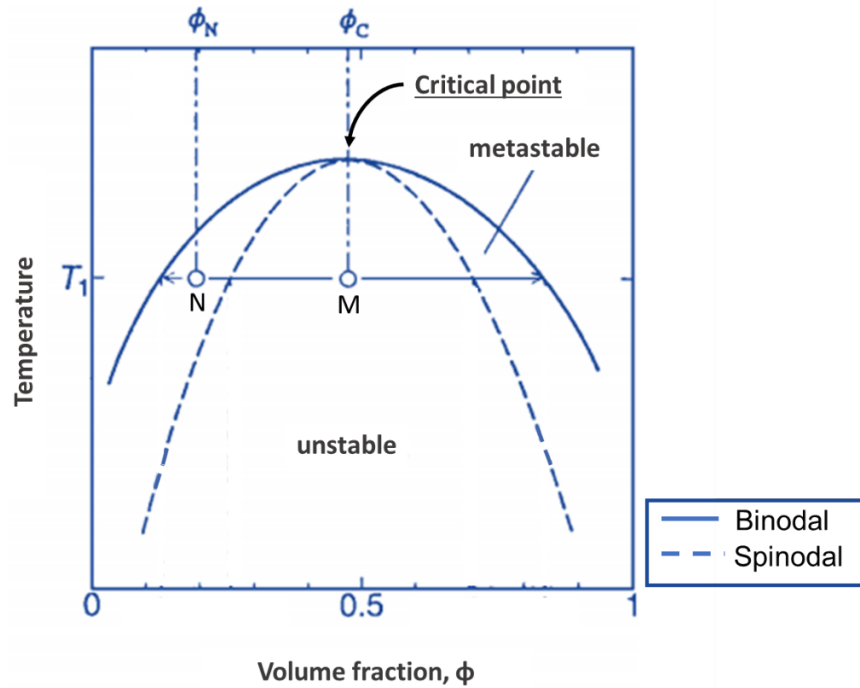
Figure 9 - Illustrative phase diagram of a binary system. Φ_C is the volume fraction of the critical composition where spinodal decomposition happens at temperature T_1. Φ_N is the volume fraction of composition where nucleation-growth happens at temperature T_1. Adapted from [23–30]

2.2. Porous materials

Due to their high surface-to-volume ratio, porous materials have taken a great deal of attention. New and different properties can be introduced in this material based on functionalization from organic and inorganic fractions. They can be applied in various fields like adsorption, catalysis, separation, life sciences, nanotechnology, etc. High surface area combined with open structure has shown that porous materials are promising in adsorption and catalysis, especially since confinement regimes and optimization of diffusion are necessary for those applications [31].

Porous materials are categorized, according to the International Union of Pure and Applied Chemistry (IUPAC) notation, into microporous (pore diameters of less than 2 nm), mesoporous (pore diameters between 2 nm and 50 nm), and macroporous (pore diameters of greater than 50 nm) [24].

Both porosity and surface area are essential properties since it influences the macroscopic properties of the solid. Porosity is defined as the ratio between pore volume – void or unoccupied space in materials – and the volume occupied by the matrix, particles, or powder [32]. In its turn, the surface area is linked to porosity since the material's surface can be porous depending on the production method. Besides that, the surface area also relies on the size and shape of the materials/particles [31,32]. Nevertheless, according to the application intended, many other structural properties may be considered. Table 1 shows the structural properties requested for materials depending on their application.

Table 1 - Porous materials applications and correspondent structural properties. Adapted from [23,27,29]

Application	Structural properties required
Energy conversion and storage	· Porous hierarchy; · High surface area; · Short diffusion length.
Catalysis and photocatalysis	· Porous hierarchy; · High surface area; · Tunable pore size · Large pore volume.
Adsorption and separation	· High surface area; · Precise pore structures and surface properties.
Sensing	· Porous hierarchy; · High surface area; · Short diffusion length.
Biomedicine	· Porous hierarchy; · High surface area; · Large pore volume.

By analyzing Table 1, the importance of hierarchically porous materials is remarkable, which involves single architectures of multiple porosities from micro-, meso- to macro- scope [29,32], being possible to synthesize bimodal micro-mesoporous, double mesoporous, macro-mesoporous and trimodal porous architectures [30,33–35].

2.2.1. Hierarchically porous materials

Hierarchically porous materials have significant interest due to their unique characteristics, including multiple levels of porosity, pore consistency at each level, highly interconnection between levels of porosity, sizeable accessible space, high surface area, low density, and excellent volume change accommodation, which confirms their diversity for employment in the most expansive applications [5,23,29,32].

The formation of multilevel porous structures provides distinctive properties depending on the arrangement and combination of pore sizes. Micro- and mesopores, due to high surface area and pore volume supply size and shape selectivity, encourage interactions between the scaffold and the active sites. However, mass transfer is diffusion-dominated, making them suitable for catalysis and separation of small molecules only. For large molecules like polymers and proteins, the diffusion rate is low, leading to a hard interaction between the architecture and the active sites and consequently catalysis and separations with low efficiency. On the other hand, macropores make mass transport easier, which means the transport limitations of the material are reduced, favouring the accessibility to the active sites.

Macroporosity may arise problems of low surface area and mechanical strength, which are indispensable for the applications of hierarchically porous materials since it preserves the scaffold's structure [29].

The rising need for materials with controlled porosity due to their improved performances, seeking the application in diverse areas, has led to the production of hierarchically porous materials through several strategies, including chemical approaches, physical-chemical approaches, and other chemical-related engineering techniques [5]. In terms of the template used (or not used), Figure 10 illustrates the synthesis routes for hierarchically porous materials fabrication. The methods involving templates confer tunable pore size and designable pore shape to the hierarchically porous structures, but a template-removal process is necessary, which turns them into more complex approaches that require more resources. Whereas the free templating methods, directly related to the spontaneous formation and self-assembly processes, are much more straightforward, but with the drawback of rough control of the pores' size and shape owing to spontaneous formation feature. The desired design is conditioned by the method or method combinations chosen. Some of the properties that the fabrication process can establish are [29]:

- Structures' porosity – generally by a combination of various approaches;
- Macroscopic morphology – films, monoliths, particles, foams, etc.;
- Functionality – e.g., hybrid materials can be fabricated to produce specific materials with the benefit of the finest properties of each component and to reduce or eliminate their shortcomings;
- Flexibility – the required porous architectures and morphologies can be applied in energy, environment, and living science fields.
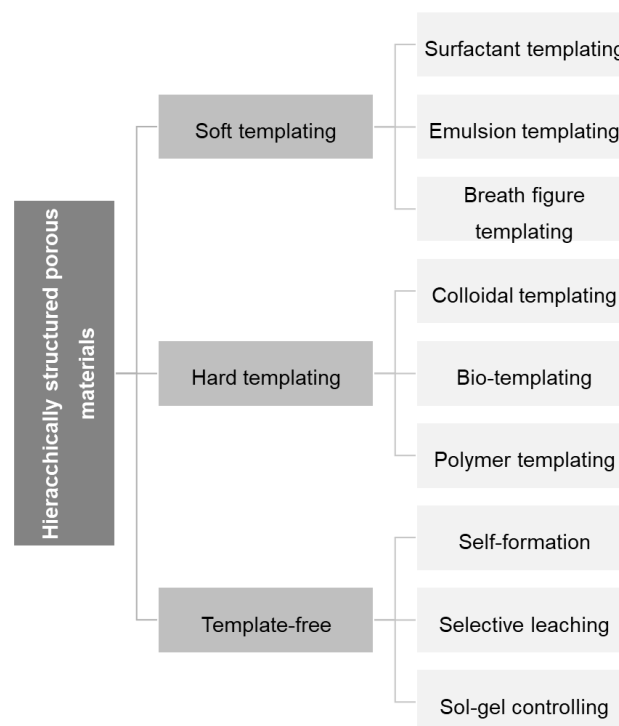
Figure 10 - Scheme of synthetic methods of hierarchically porous materials according to the template used. Adapted from [35,36]

2.2.1.1. Hierarchical porosity and alkoxysilanes

There is a substantial interest in assembling porous materials with bi- and multi-modal porosities, mainly improving their mass transfer efficiency. Thereby, the produced material takes sides of the combination of micro-, meso- and macroporosity benefits, which were referred to in the previous chapter. Hierarchically porous silicas with penetrable macropores and mesopores have been reported [37]. This combination of pore size regimes within the silicas makes them materials with a high surface area for interaction coming from the mesopores, and faster mass transport and high accessibility is guaranteed from the macropores [26,33,36]. Hierarchically meso-macroporous silica materials can be formed by the sol-gel processing attending induced phase-separation. In systems involving alkoxysilane-based gels, phase-separation can be induced using organic polymers, polar organic solvents, or strong acids [38]. The phase-separation happens because of the variations in polarity and miscibility caused by the hydrophobic siloxane species formed during the condensation's reactions and, eventually, the structure frozen. This approach is a chemical method that can be used to manufacture hierarchically porous materials, not just silica-based ones, but also to produce inorganic and inorganic-organic hybrid monoliths [17,26,36,39]. Most of the silicas are in the form of bulky monoliths or thin films, but particulate spheres may be preferred since they can be easily packed into the existing reactors or columns. [38]

2.2.1.2. Phase-separation in sol-gel systems

Nakanishi et al. (1991) [38] were the ones to present for the first time silica hierarchically porous monoliths with interconnected macropores in their skeleton. The mechanism for it was through sol-gel chemistry attending phase-separation through spinodal decomposition by achieving gelation at the spinodal decomposition process's transient state.

Phase-separation thermodynamics

Flory-Huggins theory allows the understanding of the thermodynamics of the phase behaviour of a two-component system. This theory is based on the free Gibbs energy change of mixing (Equation 4) considering a lattice model, leading to the Flory-Huggins equation (Equation 5), wherein the first two terms inside the parenthesis express the entropic contribution and the last term the enthalpic contribution [14,22,33,40].

$$\Delta G_m = \Delta H_m - T\Delta S_m \tag{4}$$

$$\Delta G_m = kT\left[\frac{\phi_A ln\phi_A}{N_A} + \frac{(1-\phi_A)ln(1-\phi_A)}{N_B} + \chi_{AB}\phi_A(1-\phi_A)\right] \tag{5}$$

ΔG_m represents the free energy of mixing, ΔH_m the enthalpy of mixing, T is the absolute temperature, ΔS_m is the entropy of mixing, N_A and N_B are the number of statistical segments (related to the degree of polymerization) of hypothetical polymer A and solvent B, respectively, ϕ_A is the composition of the polymerizable species A, k is the Boltzmann constant and χ_{AB} is the dimensionless interaction energy parameter or Flory interaction parameter [41].

As shown in Equation 5, the free energy of mixing is a function of the composition, and its dependence can be visually analyzed, resorting to Figure 11. By fixing a single temperature, with at least two minima, it is observed that the binodal points correspond to where ΔG_m reaches its minimum, i.e., when the first derivate of the Flory-Huggins equation is zero (Equation 6), and the spinodal line corresponds to the inflexion points of the ΔG_m curve, so when the second derivate is zero (Equation 7).

$$\left(\frac{d\Delta G_m}{d\phi_A}\right) = 0 \tag{6}$$

$$\left(\frac{d^2\Delta G_m}{d\phi_A^2}\right) = 0 \tag{7}$$

Phase-separation of a polymer happens when polymer molecular weight, solvent composition, or temperature changes are verified since it results in changes of interaction energy parameter, leading to new binodal points [22].

If the curve of ΔG_m (Figure 11) is concave or convex without inflexion points, the components will completely mix into one phase. When the free energy mixing curve has two or more inflexion points, solutions with compositions between two points where $\frac{d^2\Delta G_m}{d\phi_A^2} < 0$ – free energy mixing curve in that range is concave downwards – are solutions inside the unstable region so phase-separation occurs spontaneously through spinodal decomposition. Whereas solutions with compositions between two binodal points where $\frac{d^2\Delta G_m}{d\phi_A^2} > 0$, are metastable solutions, and the thermal fluctuations in the composition are silenced due to the creation of an energetic barrier, so phase-separation takes place by nucleation-growth [22].
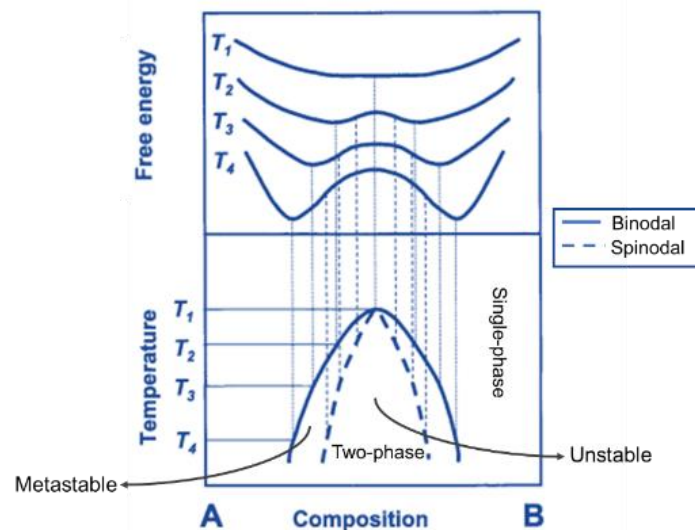
Figure 11 – Illustration of how the energetics of the system influences its phase diagram. Adapted from [14,22]

In the phase diagram, the point where binodal and spinodal phases overlap is the critical point or critical value of the Flory interaction parameter. Hence, it is related to the mixture's temperature, and it defines the lowest or highest temperature in which the solution can phase separate:

- Upper critical solution temperature (UCST) – critical temperature above which the components of a mixture are miscible in all proportions;
- Lower critical solution temperature (LCST) – critical temperature below which the components of a mixture are miscible for all compositions.

Critical point stand by the third derivative of the Flory-Huggins equation, and resolving it, a reliance on the degree of polymerization of both components is stated:

$$\phi_C = \frac{\sqrt{N_A}}{\sqrt{N_A} + \sqrt{N_B}} \tag{8}$$

Miscibility exists when Gibbs's free energy change of mixing is negative, so when it turns from negative to positive, phase-separation happens due to thermodynamics driven force. Concerning spinodal decomposition, in Figure 12 (i), the arrow pointing down indicates a fast decrease in the solution temperature; thus, a decrease in the degree of freedom between species and subsequently phase-separation is induced – physical cooling or physical quenching. Figure 12 (ii) shows a polymerization–condensation reaction on course, i.e., a reduction of the ΔS_m value due to formation of oligomers moving the critical point (Equation 8) in the diagram, which also leads the system into the two-phase region – chemical cooling or chemical quenching [14,37,38,40].
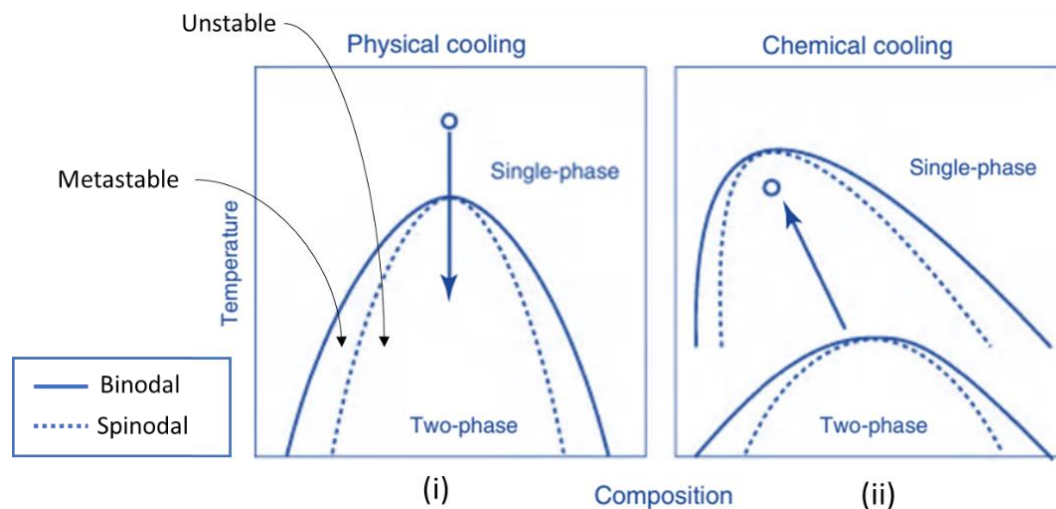
Figure 12 - Illustrative phase diagrams of systems with immiscibility window for comparison of physical and chemical cooling. Adapted from [42,43]

Regarding the pore structure, interconnected macroporosity can be achieved by controlling the volume fractions of the gel-rich/solvent-rich phases and gelation time, as Figure 13 suggests. Besides that, supramolecular templating, or appropriate gelation treatments, such as hydrothermal treatment or pH conditions, are other ways to tailor the micro-mesopore structure [21].
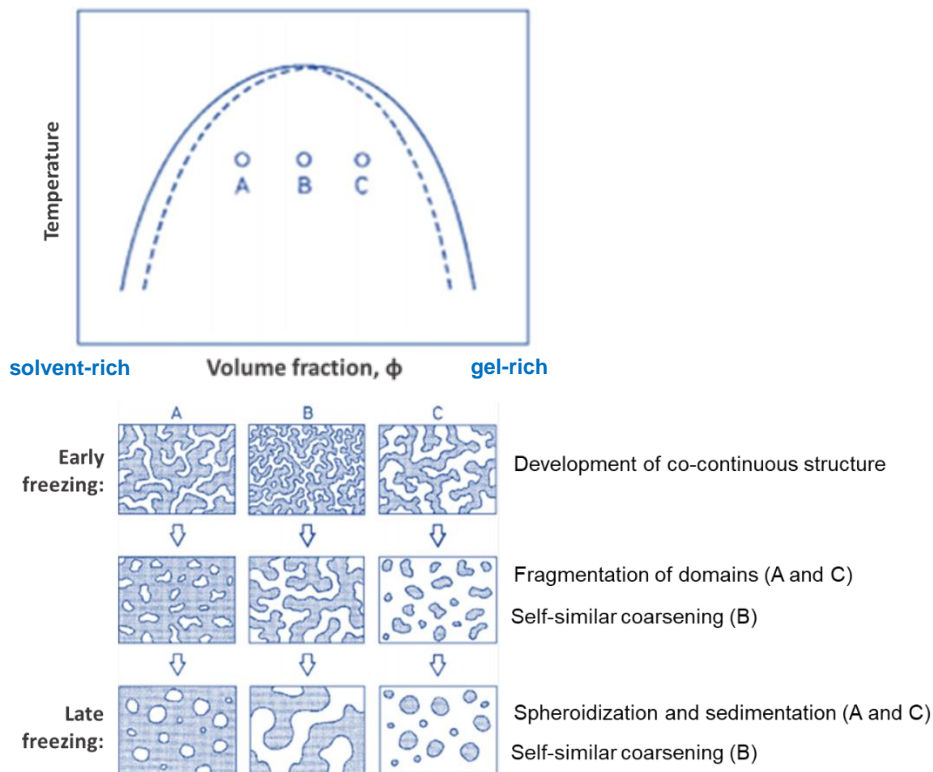
Figure 13 - Illustration of the coarsening evolution at different volume fractions of gel-rich/solvent-rich according to the time in the unstable region relative to spinodal decomposition. Adapted from [39,44]

2.2.2. Hybrid porous materials

Hybrid materials consist of two moieties combined on the molecular level, and usually, those moieties are inorganic and organic components. Their big advantage is that this combination allows the material to benefit from the properties of both organic – structural flexibility, ease of processing at low temperature – and inorganic constituents – thermal, chemical, and mechanical stability, hardness – in *one* structure [17,39]. A practical example is when in sol-gel materials, a more hydrophobic material is required. The hydrophobicity molecular components can be improved if alkyl- or aryl-substituted trialkoxysilanes are introduced in the formulation. This way, a material with multifunctionality, not available otherwise, is formed. In porous hybrid materials, the objective is to accomplish a synergy between the porous inorganic framework's original properties and the organic units' properties. [39].

Hybrid materials are classified based on their interface bonding: class I hybrids – organic and inorganic units are intimately combined with weak or no bonds (hydrogen, van der Waals, or ionic) – and class II hybrids – the combination is done by strong chemical interactions (covalent or ionocovalent) [17].

There are two typical approaches to the formation of hybrid materials [39,44]:

- Building block approach – well-defined building blocks (e.g., organic clusters or nanoparticles) reacting to form the hybrid material. The main advantage of this method is the fact that the precursors do not suffer significant alterations. Part of the original integrity exhibited in the

precursors is kept in the final hybrid material what leads to a better prediction of the structure properties, something that does not happen when precursors are shifted into novel materials;

- *In situ* formation of the components – here, the precursors are chemically transformed into multi-dimensional structures with different properties compared to the original structural units. The sol-gel process is the most notorious method inside this approach.

2.2.2.1. Sol-gel method and hybrid materials

Since the sol-gel method presents mild reaction conditions and is suitable for different precursor reagents, it is preferred to produce hybrid organic-inorganic materials compared to other technologies for the same aim. It also permits the inclusion of other components that may establish more functionally to the produced material [39]. The hybrid networks' final properties are determined by the ones inherent to the respective inorganic and organic compounds and the phase morphology and interfacial region between them [26,39,44,45].

Alkoxysilanes are notorious precursors for preparing organic modified materials. The chemical reactions involved have already been described in Chapter 2.1.1, as well as the significance of the reaction conditions. For example, the pH can lead to different silica networks due to the reactants' different reactivities.

The hybrid materials formation through sol-gel usually is made by organic molecules embedded into an inorganic material without chemical bonding or via covalent bonding [17,39] :

- Without chemical bonding – a dissolution of the organic molecules into the inorganic precursor solution is made, and the gel matrix is formed around those molecules entrapping them;
- Covalent bonding – the R_2 group of the organotrialkoxysilanes $R_2Si(OR_1)_3$ is linked through the hydrolytically stable Si-C bonds to the network-forming inorganic part of the molecule – co-condensation. Typically, organotrialkoxysilanes have problems obtaining a 3-D gel network, and to overcome this limitation, they are mixed with tetraalkoxysilanes since these lead to a higher degree of condensation of the prepared hybrid material.

A typical example of a not desirable phase-separation is the incompatibility between organic groups and aqueous synthesis of inorganic matrices that may result in macroscopic phase-separation during the formation of hybrid materials if the organic and inorganic moieties are mixed. To overcome this inherent problem, linking the inorganic and organic moieties in one single molecule is an option. Sill, phase-separation at the nanometre scale may occur. This type of phase-separation, which separates the solution into a hydrophilic and hydrophobic area, is sometimes purposively induced when porous materials with organized porosity are required [22,39]

2.3.   Microspheres

The terms "microspheres", "microparticles", and "microcapsule" manage to be referred to as synonymous in literature in terms of microencapsulation. Microencapsulation was defined by Ghosh in 2006 [9] as a process where micrometric-size solid particles or liquid/gas droplets are confined in an

inert shell, protecting and isolating those substances from the outside environment. As a result of this process, it is obtained microcapsules (MCs). The selected technique to form the microcapsules defines the shell's deposition process on the core material, defining its morphology. That means that it is possible to synthesize full or hollow particles [9,10]. Theoretically, microspheres (MSs) refer only to microparticles (MPs) – particles with a diameter typically between 1 and 1000 μm – in spherical shape made up of a polymeric or ceramic matrix in which active sites are found in its pores. To a better clarification of this, Figure 14 can be seen.

In general, as mentioned above, MPs – MSs and MCs – or other scaffolds in the micro range have the purpose of storing and isolating functional compounds at any physical state and release the content in a controlled way [10].

In general, to the naked eye, MPs seem to be a fine powder. The MSs can be made from polymers, silica, metal, cellulose, or other materials depending on the application. Thus, considering the method for its production – which can enable the achievement of a required morphology – each type of MSs presents distinctive properties and functionality.
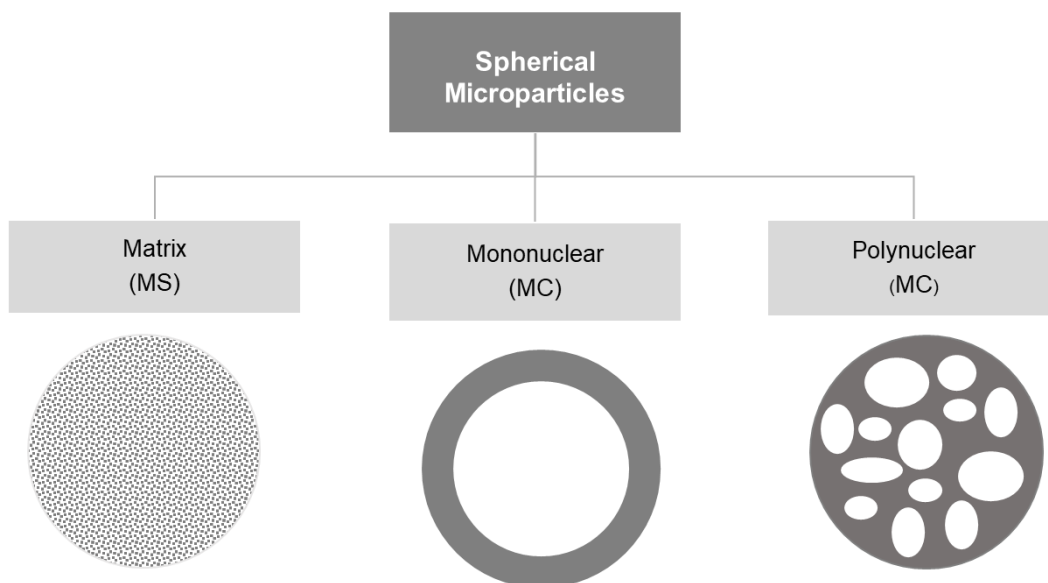
Figure 14 – Spherical microparticles morphology. Adapted from [10]

2.3.1. Production of porous silica-based microspheres: Historical context

Stöber et al. (1968) [46] described the first method to produce micron range silica spheres based on the sol-gel chemistry. This method lay on monodisperse nonporous silica spheres with sizes up to 2 μm by carrying out the hydrolysis and condensation of tetraalkyl silicates, in alcoholic solutions, using ammonia as the catalyst for the formation of particles in a spherical shape. Their investigation showed that the size of the particles obtained was not easily reproduced, but a controlled growth of uniform nano-sized spherical particles could be achieved. Van Helden et al. (1981) and Bogush et al. (1988) [47,48]

developed several studies to control the particle diameter and particle size distribution, based on Stöber's method. However, the conclusions reached were just empirical. Until this point, the particles' size distribution and morphology were dependent on reactants, especially the amount of ammonia – as the concentration of ammonia increased, the larger the particles, with a diameter up to 2 μm [49,50].

Since it is crucial to control particle morphology such as size and diameter, the pores' volume and structure are crucial aspects concerning porous microspheres' properties to employ it in specific applications. Thus, the physical and chemical processes involved in the production, concerning the influence of experimental conditions and stoichiometry of the implicated reactions, should be understood [51–54].

In terms of the production of spherical particles, Büchel et al. (1998) [55] have combined two studies with Stöber's method being able to produce submicrometric-size particles with spherical shapes and with mesopores.

In subsequent years, an attempt was made to understand the mechanisms of particle development and growth. Matsoukas & Gulari (1988) and Bogush & Zukoski IV (1991) [56,57] reported studies regarding the nucleation and growth of the particles claiming it as an aggregation of smaller particles and as a result of the addition of monomers to the reaction, respectively. Still, these studies only allowed the growth of seeded sub-micron particles [51]. The particles' porosity is not a concern in these studies, although Bogush & Zukoski IV (1991) were able to produce silica particles with a porosity of (only) 11-15% of the total particle volume [58]. Nonionic polymer and alkylamine surfactants have been used as templates to adjust the silica particles' internal structure and size [58–60].

Thus far, besides the approaches based on Stöber's method, several other synthesis methods have been used to prepare silica MSs, including template methods, spray drying, micro-emulsion method, and other sol-gel methods. By the template method, with a cationic surfactant as a template – e.g., alkylamines –, it was likely to produce mesoporous silica particles with a pore diameter up to 4 nm while using a block copolymer – nonionic polymer – as a template, the size of the pores could be increased up to 11 nm even though there were problems of secondary nucleation and agglomeration. By employing spray drying, these problems could be overcome, but a vast particle size distribution was obtained, meaning that size classification is required and, consequently, more cost and lower yield [61–66].

Since Stöber's method, the sol-gel method has been used to form various types of inorganic materials. Nowadays, by combining different methods, there are multiple ways of producing spheres with different nanometres in size, either porous or nonporous. Sol-gel technology alongside the microemulsion template has been proven to be the most economical and practical approach for MSs and other matrices' production since it permits the synthesis of inorganic and hybrid structures and operates at mild conditions [2,67].

2.3.2. Porous silica-based microspheres

In the last decades, inorganic matrixes as silica MSs have been receiving much attention. Since silica has excellent chemical resistance, thermal stability, biocompatibility and is non-toxic for the environment and comparing to polymer-based MSs, the latter cannot typically be employed in certain conditions, since they have lower chemical and physical stability [10,68]. Thus, silica MSs have broad applications in several fields such as ceramics, catalysis, chromatography, electronics, cosmetics, coating materials, drug delivery, and so on [10,67]. For those applications, controlling the particle size and the pore size of silica spheres is very important and depending on the method for their production, it is possible to produce microporous (≤2nm), mesoporous (2–50nm), or macroporous (≥50nm) silica MSs [3]. Porous silica MSs, as functionalized micro scaffolds, have the character of containers being qualified to work as supports of nanoparticles or active sites and carriers of substances. Therefore, this type of MSs are excellent material for controlled release and separation, or scaffolding applications [67].

2.3.3. Sol-gel/Micro-emulsion process

For the production of silica MPs with designable size and porosity, various methods have been reported, such as soft- and hard-template methods (Table 2 presents organic templates according to the resultant porosity in MSs), spray-drying, and polymerization-induced colloidal aggregation. Since multifunctionality is a foremost requisite when preparing porous materials, either entrapment or controlled release may be capabilities to consider when producing silica MSs due to the specific microstructure that those imply. Sol-gel chemistry permits the production of silica matrices at low temperatures while the control of microstructure is possible. So, approaches like spray-drying and emulsion polymerization are used wherein microdroplets are confined reaction vessels for sol-gel reactions to happen [11,12]. However, spray-drying only leads to the formation of 7-12nm pores in particles of large size distribution, so the sizes have to be classified, meaning more costs and low yield, as was mentioned before in Chapter 2.3.1. Emulsion polymerization seems to be the solution to those limitations, in which the medium is a microemulsion [10].

Table 2 - Porosity according to the organic template chosen [10].

Soft template	Small organic molecules	Micelles, liquid-crystals, block-copolymers	Microemulsions
Type of porosity	Microporosity	Mesoporosity	Macroporosity

2.3.3.1. Microemulsion technology

Microemulsions are considered lyophilic colloids, like micelles. They are isotropic and thermodynamically stable systems with tiny droplets [7,11,69]. The differences between macroemulsions and microemulsions rely on the former having larger droplets than the latter and the amount of surfactant used (10–40% in microemulsions and 1–2% in macroemulsions). There are three types of microemulsions according to their behaviour, established by the Winsor classification system [11,69]:

- Type I – refers to O/W microemulsions, in which the oil phase is solubilized within the continuous water phase;
- Type II – refers to W/O microemulsions or reverse microemulsions, in which the water phase is solubilized in the oil phase;
- Type III – refers to systems in which the water phase and oleic phase are in equilibrium with a surfactant leading to a mutually interconnected microstructure between the aqueous and oleic phases represented in Figure 15 by the hatching in single-phase. These emulsions can be considered as bi-continuous.
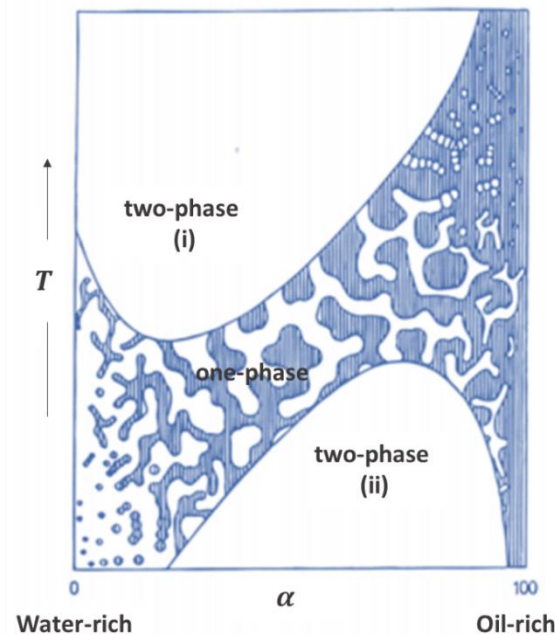
Figure 15 - Illustrative diagram for the behaviour of oil/water/surfactant ternary mixture, for a constant surfactant concentration according to weight fractions (α) of water and oil and temperature (T). Adapted from [11]

Observing Figure 15, there are a one-phase region and two two-phase regions. In the one-phase region, where the mixture is macroscopically homogeneous but microscopically heterogeneous, there is an O/W microemulsion on the water-rich side (type I), W/O microemulsions on the oil-rich side (type II), and type III microemulsions in the middle (at circa 30-70 wt %). The two-phase (i) is where W/O microemulsion coexists with an aqueous phase and the two-phase (ii) where O/W microemulsion coexists with an oleic phase.

There are systems in which a fourth component, a cosurfactant, is added to the microemulsion (oil/water/surfactant system). This cosurfactant leads interfacial tension to almost zero values, which directs to almost spontaneous emulsification. An example of a cosurfactant is long-chain alcohols.

By employing a combination of sol-gel chemistry with microemulsion technology as a template, microspherical particles can be prepared, and a careful choice of solvent and surfactants is essential. In this approach, emulsion droplets work as micro-reactors, where the polymerization reaction will take

place [70]. Since microemulsions are dynamic systems, and the microemulsion droplets continuously collide with one another, so in the process, there are exchanges of the content of their aqueous core. The size of those droplets will determine the microparticle size, and for its turn, it is a function of emulsion parameters, such as the nature of the surfactant and solvent, water/surfactant ratio, and the presence of a cosurfactant [11].

As previously mentioned in Chapter 2.1.2, the HLB value may be considered when choosing a surfactant. W/O emulsions require affinity for oil (lipophilic), and the recommended values are 3-8, while O/W require affinity for water (hydrophilic), and HBL values may be in the range 8-18 [10]. Table 3 presents some surfactants that can be used and their respective HBL value.

Table 3 - HLB values for some surfactants. Adapted from [10,69]

Surfactant	HBL
Sorbitan tritearate (SPAN 65)	2
Sorbitan monooleate (SPAN 80)	4
Diethylene glycol monolaurate	6
Sorbitan monolaurate (SPAN 20)	9
Polyoxyethylene (10) cetyl ether (BRIJ 56)	13
Polyoxyethylene sorbitan monooleate (TWEEN 80)	15
Sodium dodecanoate	21
Sodium octanoate	23
Sodium heptadecyl sulfate	38
Sodium dodecyl sulfate	40

For the sol-gel with emulsions as templates (for MPs production), ionic and nonionic surfactants act as pore formation agents due to their solubilization properties, so their concentration and nature will determine the pore size. For example, Tween 20 is associated with water and silicates by hydrogen bonding, leading to larger pores and thicker shell walls, while increasing the concentration of Span 80 will decrease the pore size distribution.

2.3.3.2. Porous silica microspheres, microemulsion, and the sol-gel technique

When manufacturing silica MSs, alkoxysilane precursors are utilized in the sol-gel reaction according to what has been already stated at the beginning of Chapter 2.1.

In most cases, W/O emulsions are exploited to form porous microparticles, wherein the dispersed water droplets act as isolated compartments for reactions. These particles may be full or hollow (MSs or MCs,

respectively), which is a feature related to the addition sequence of the chemicals involved in their preparation. The sol-gel emulsification must happen along with the gelation to MSs attainment. To that matter, the sol-gel solution is mixed with an emulsifier solution in a solvent, water, and alcohol to drive emulsification. The immiscibility of the apolar solvent (oleic phase) with the polar sol-gel solution is what leads to the development of a confined reaction vessel wherein hydrolysis and condensation will occur for further gelation and eventually the formation of porous MPs [10,70].

Equations 2 and 3 describe the hydrolysis and condensation reactions involved in the manufacture of MSs, and as it has been said, pH is one determinant parameter to manage their inner morphology. As Figure 2 suggests and considering what has been reported [70], hydrolysis is fast under acid catalysis conditions; condensation is the rate-limited step, and dissolution reactions are hindered. Hence, silica particles' growth in microemulsions' droplets is done by slowly consuming all hydrolysed precursors, originating small microporous MPs that will aggregate into larger particles. Moreover, for the same approach as described before, when at basic catalysis, there is a big range of pH values wherein the dissolution reactions are endorsed, and condensation is promoted relatively to hydrolysis. Thus, a faster condensation against slower hydrolysis causes a rapid consumption of precursors. The ripening of potential aggregates and a high dissolution rate lead to spherical particles' production with negligible porosity [22]. This mechanism is explained by nucleation-growth phase-separation through heterogeneous nucleation [10].

These porosity limitations can be overcome by the "two-step" sol-gel polycondensation process, in which the hydrolysis firstly occurs under a low pH followed by condensation at higher pH. Therefore, better control of the sol-gel reaction is achieved since hydrolysis can develop entirely. For what is concerned, through this approach, only mesoporous MSs have been produced [10].

2.3.3.3. Porous silica microspheres by induced phase-separation

As stated before, phase-separation by spinodal decomposition accompanied by the sol-gel technique has allowed the production of highly porous hierarchical monoliths (e.g. Kaji et al. (1993) [20]). Although porous MPs have been successfully formed and spinodal decomposition has been well investigated, porosity control in MSs has not been totally studied. Recently, M. Vale et al. (2020) [1] published the first report about this matter, which is the dissertation's framework. In that report, contrarily to Kaji et al. (1993) [20], no gelation mediation agent is needed since the use of GPTMS precursor provides an oxirane group, that by its opening, leads to the increase of the degree of polymerization (for silica domains) and therefore, acts as an inherent gelation promoter. Besides, the phase separation by spinodal decomposition happens inside the aqueous droplets of a W/O emulsion (microreactors), so not in the bulk form, like reported by Kaji et al. (1993) [20].

2.4. Photocatalytic systems

Photocatalytic systems involve a photocatalytic process: an improved oxidation technique in which a catalyst accelerates a chemical reaction when exposed to light. It allows the elimination of all types of

contaminants, such as bacteria, hazardous substances, pharmaceuticals, and organic pollutants by photodegradation [71,72].

Regarding the reactants' physical state, photocatalysis comprises two forms: homogeneous and heterogeneous photocatalysis, in which the semiconductor and reactant are in the same phase or different phases, respectively [72,73]. The latter comprises a semiconducting substance as a photocatalyst, i.e., it is chemically activated under radiation. This process's principle is a semiconductor illuminated with light at a wavelength equal to or greater than its bandgap, so photons are absorbed. It induces the changeover of electrons from the valence band (VB) to the conduction band (CB), leaving a positive hole in the VB. It is the formation of this charge carrier that allows reduction and oxidation of different compounds (which will act as donors or acceptors), not essentially adsorbed on the photocatalyst's surface [74].

Photocatalysis is a huge potential technique since it is suitable for antifouling, energy storage and conservation, self-cleaning, air purification, wastewater treatment, etc. In terms of water treatment, it comprises the removal of molecules determined as pollutants and can be performed by (i) the adsorption of those molecules on the surface of an active element. Although adsorption demands the reactivation of the adsorbent, making this process discontinuous; (ii) reverse osmosis wherein a semipermeable membrane filters the contaminants molecules, but membrane regeneration is also demanded; (iii) the on-topic photocatalysis which is performed through a catalyst that chemically turns the pollutant molecules into less active species [71].

Semiconductors, due to their electronic structure, work as catalysts in photocatalysis processes. Metal oxides and several other compounds have been studied and applied in photocatalysis as semiconductors. From the metal oxides, titanium dioxide (TiO_2) is the most common due to its ability to be active at the visible light wavelength (most of the reports use ultraviolet light as radiation), providing the best balance between absorption of the photons, cost, chemical and photochemical stability, and lack of toxicity. Even though some drawbacks can be pointed [75]:

- The semiconductor as active species in general, and TiO_2 included, are mostly used in nanoparticle form, and their appliance relies on dispersion into the media intended to purify, requiring a subsequent removal step. It indeed permits a higher contact between the semiconductors and the contaminants, but ultrafiltration is needed after the photodegradation to remove the nanoparticles;
- The previous technique can only be performed in discontinuous, allowing only the treatment of small volumes.

Such drawbacks enhanced the need for tailored porous materials, to act as scaffolds (support) for those nanoparticles, leading to the study and design of meso-macroporous silicas where the sol-gel method has been the most investigated technique. On the other hand, to incorporate nanoparticles (NPs) in photocatalytic systems, in-flow reactors have to be developed, since usually slurry reactors apply TiO_2 in suspension.

To overcome the presented limitations, different supports for the NPs have been used, and regarding silica materials as supports, there are two strategies to incorporate NPs within the matrix:

- Directly addition of the precursor; for TiO_2 NPs it comprises the addiction of Ti alkoxides directly to the silica sol-gel reaction medium;
- The addition of the NPs after the solid silica network is formed by deposition, impregnation, atomic layer deposition, or others.

The supports must be mechanical and thermal resistant, with a high surface area to enable loading of the NPs and sites in its structure for covalent binding so NPs can be attached. Silica materials are very suitable materials as supports, mainly because they are transparent in the UV-vis region, and it does not interfere with the generation of charge carriers in TiO_2.

In applications such as photocatalysis and catalysis, hierarchically porous materials can act as (photo) catalysts or (photo) catalyst supports since their catalytic performance is improved. As microscaffolds (support materials), they provide the surface area necessary for high dispersion of active components (metals, metal oxides, enzymes, or other species). As catalysts, their porosity modality allows separation of reactants due to the size and shape selectivity of mesopores. When developing these microscaffolds, macroporosity is a critical feature to consider because it improves the in-flow properties of the media to purify, since macropores work as a mass transport system for liquids and gases, increasing the accessibility of the smaller pores and promotes the interaction with the photocatalytic NPs [75].

3. Materials and Methods

3.1. Materials

Ammonia (Merck, 25% w/w), Decahydro-naphthalene for synthesis (Decalin, a mixture of isomers cis and trans, Merck, 98%), (3-Glycidoxypropyl)trimethoxysilane (GPTMS, Xiameter OFS-6040, Dow Corning, >98,5%), Hydrochloric acid 37% (HCl, Carlo-Erba), SPAN 80® for synthesis (Merck), Tetraethylorthosilicate (TEOS, Sigma-Aldrich, 98%), bidistilled water and Aeroxide® P25 commercial TiO_2 nanoparticles (Evonik).
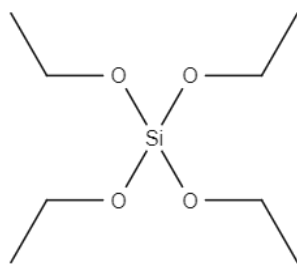
Figure 16 - Molecular structure of the TEOS precursor.
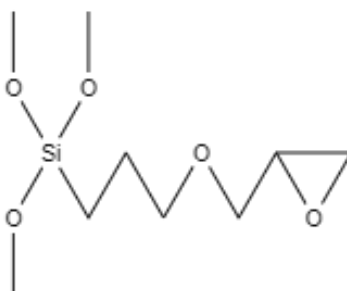
Figure 17 - Molecular structure of the GPTMS precursor.
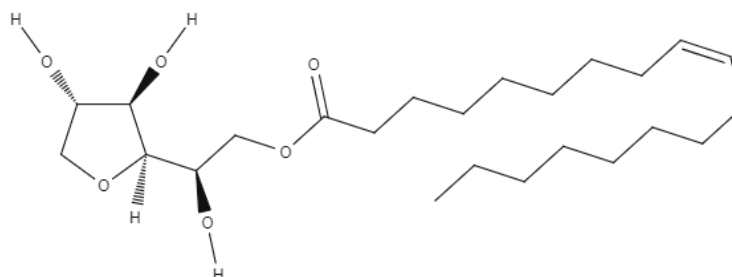
Figure 18 - Molecular structure of SPAN 80.
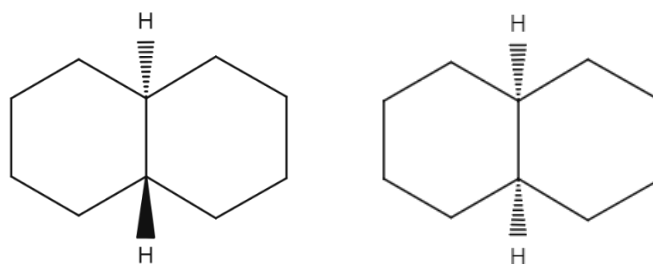
Figure 19 - Molecular structures of decalin isomers trans (left) and cis (right).

3.2. Experimental procedure for porous MSs production

Two main methods were assessed for the synthesis of the silica microspheres, and with these two methods, several studies were made. These two methods differ in the way condensation is promoted: pH promoted, and temperature promoted. Both methods require the same initial steps, the pre-hydrolysis, and the emulsification, being the different step the sol-gel reaction, where the condensation occurs.

1-   Pre-hydrolysis of silica precursors

To the pre-hydrolysis, 20 g of TEOS, 20 g of GPTMS, and 15 g of an aqueous solution of HCl (0,05M) (proportion of 1:1:0.75 (w/w)) were mixed in a plastic cup (Figure 20 (i)) at 50-100rpm for 50 minutes at room temperature (Figure 20 (ii)). Then 300 µL of HCl (37%) was added (Figure 20 (iii)), and the stirring was finished 10 minutes after this addition obtaining the pre-hydrolysed silanes solution (Figure 20 (iv)). The pre-hydrolysed solutions' viscosity measurements were made using a Brookfield Viscosimeter DV-II+ Pro equipped with a CP40 spindle at 30 rpm.
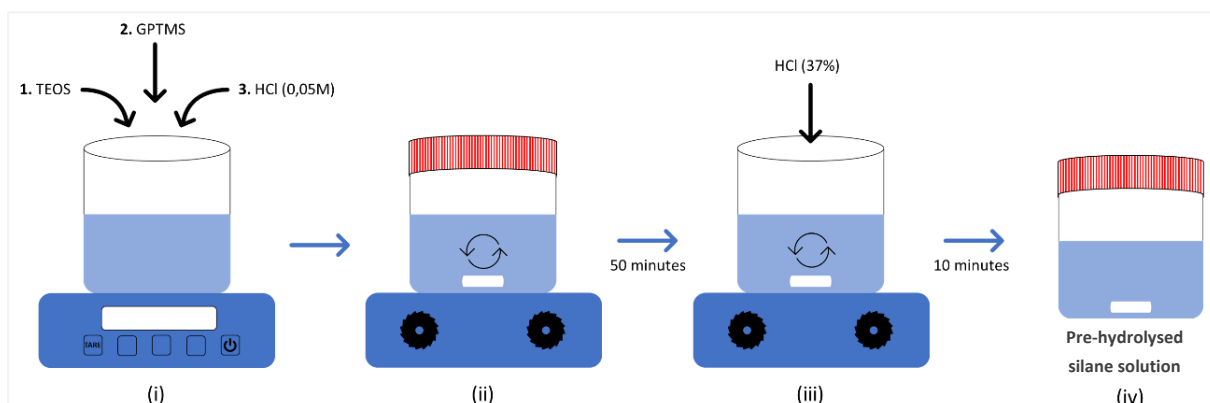
Figure 20 – Illustrative representation of the pre-hydrolysis step.

2-   Preparation of the W/O emulsion

To the emulsion, 100 g of decalin and 6g of SPAN 80 (the emulsifier) (proportion of 100:6 (w/w)) were mixed (Figure 21 (i)), with vigorous stirring of 18000 rpm, using IKA T18 digital ULTRA-TURRAX®, for 3 minutes (Figure 21 (ii)). Then 45 g of bidistilled water was added (Figure 21 (iii)), and the resultant mixture was stirred for 10 minutes (Figure 21 (iv)).

It is also important to refer that both steps, the pre-hydrolysis of silanes and the emulsion preparation, were managed to end simultaneously, to guarantee reproducibility and no change of properties.
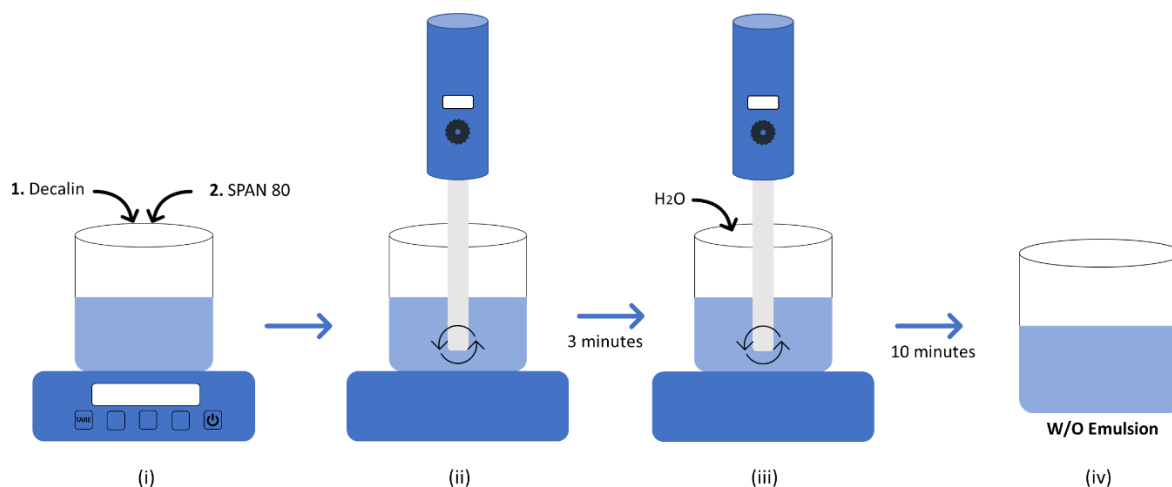
Figure 21 - Illustrative representation for the emulsion preparation.

3- Reaction and filtering/drying

Condensation stimulated by pH

Firstly, the emulsion was introduced inside the reactor with a stirring of 600 rpm (Figure 22 (i)), and the pre-hydrolysed solution was added to this emulsion dropwise for about 30 minutes to 1 hour (Figure 22 (ii)). After this, the resultant solution was maintained for 15 minutes at room temperature and 600 rpm for stabilization. Then a specific temperature was fixed (65, 75, 80 and 85 °C) (Figure 22 (iii)), and condensation was induced by the addition of 75 µL of ammonia (25%) every 15 minutes until the solid MSs were formed (Figure 22 (iv)). Lastly, the reaction product was filtered under vacuum and with acetone (Figure 22 (v)) and dried at 45 °C for 24h (Figure 22 (vi)).

Condensation stimulated by temperature

After adding the reactants into the reactor (Figure 23 (i) and (ii)), a temperature profile was established with specific times according to Table 4 (Figure 23 (iii)). When solid MSs were formed, the reaction product was filtered under vacuum and dried at 45 °C for 24h (Figure 23 (iv) and (v)). Besides that, the effect of the rate of addition of the hydrolysed silanes was also studied.

Table 4 – Temperature profile applied during the sol-gel reaction to stimulate condensation.

Temperature (°C)	Time (min)
T_{room}	60
65	60
70	10
75	15
80	60
85	30-60
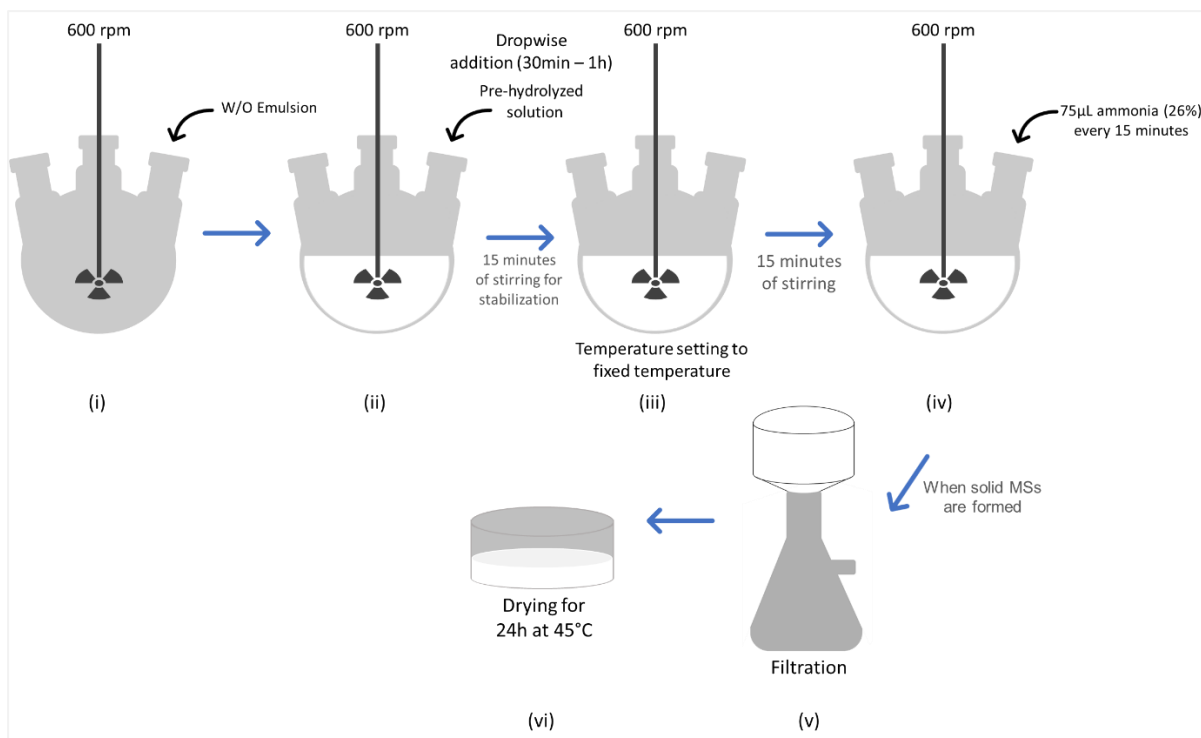
Figure 22 – Illustrative representation of the sol-gel reaction when condensation is stimulated by pH.
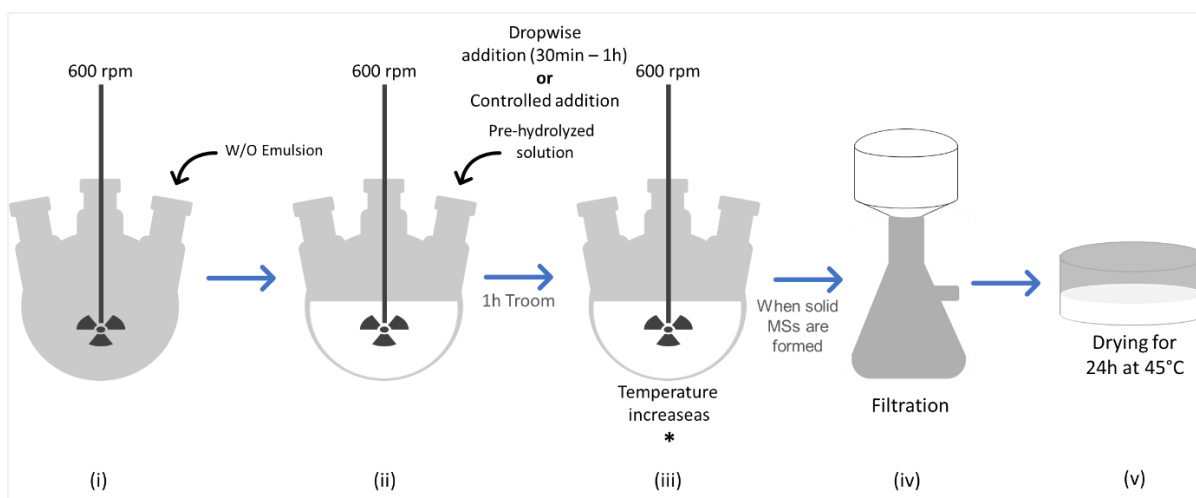
Figure 23 - Illustrative representation of the sol-gel reaction when condensation is stimulated by temperature. The asterisk (*) denotes the temperature profile described in Table 4.

3.3.   NPs immobilization process

Firstly, about 500 mg of the MSs "powder" were subjected to 900 ºC for 30 minutes to remove possible remained water from the synthesis or gained due to air humidity at some point of its handling, as well as to eliminate organic compounds from its composition.

The impregnated NPs in the MSs were Aeroxide® P25 commercial TiO_2 nanoparticles, and the process was made according to the following:

- Approximately 200 mg of MSs were mixed with 35.6 mg of NPs in 1.3 mL of water and sonicated for 10 min;
- The now loaded MSs with NPs were dried for at least 15h at 45 ºC;
- For guarantee, the dried loaded MSs were subjected to 500 ºC for 1 hr to remove the humidity that could have remained through the immobilization process and to promote the establishment of covalent bonds between Ti-OH from P25 NPs and Si-OH groups at the surface of the MSs.

3.4.   Characterization of the porous microspheres

The obtained MSs' characterization in some successful experiments was carried out through the following:

- Fourier transformed infrared spectroscopy (FTIR) by attenuated total reflectance (ATR) – for the study of the molecular structure of the MSs, as well as the presence of NPs in the MSs;
- Scanning Electron Microscopy (SEM) – for achieving photomicrographs to assess the morphology, size distribution, and porosity of the MSs;
- Energy-dispersive x-ray spectroscopy (EDS) – for determination of the elementary composition of the MSs and confirmation of P25 NPs on the MSs;
- Thermogravimetric Analysis (TGA) – for verification if there were remained organic groups and humidity in the MSs with the NPs immobilized.

FTIR- ATR spectra were obtained using a Perkin Elmer, Spectrum Two, FTIR spectrometer with a UATR Two accessory, at a resolution of 4 cm^{-1} and 8 scans of accumulation. TGA analysis was conducted under a nitrogen atmosphere (100 mL/min), using a Hitachi STA7200 Thermal Analysis System equipment, in a range of 45-600 ºC at a temperature rate of 10 ºC/min. Lastly, the SEM photomicrographs were obtained using Hitachi S2400 microscope with an EDS Bruker light elements detector attached (a 15 mm layer of gold-palladium was sputtered on the samples before observation, using a turbomolecular pumped coater Q150T ES from Quorum Technologies).

4. Results and Discussion

4.1. Porous microspheres formation

It should be mentioned that there are two systems to consider: the emulsion system as a whole and the system within the water droplets.

Throughout the synthesis of the porous MSs, different parameters relative to the described methods were varied. The results are divided into the following features:

- Pre-hydrolysis' conditions;
- Emulsion's conditions;
- Formation of the MSs: stimulating condensation by pH;
- Formation of the MSs: stimulating condensation by temperature:
    - Quantity of silanes;
    - Quantity of SPAN80 in the emulsion;
    - Controlled addition rate of pre-hydrolysate to the emulsion;
- The viscosity of the pre-hydrolysed solution;
- Characterization of the successfully produced MSs;
- Immobilization trials of TiO_2 NPs within the MSs.

4.1.1. Pre-hydrolysis of the silica precursors

TEOS and GPTMS were the utilized silica precursors for carrying out the MSs formation. The former's inorganic character provides chemical and mechanical resistance and network formation capabilities, and the latter's organic character (glycidyloxy group) provides chemical functionality and mechanical compliance to the scaffolds. This way, hybrid MSs can be produced.

When the TEOS and GPTMS precursors were mixed with water, a two-phase solution was immediately formed because of their immiscibility. At the beginning of the stirring, the formed emulsion showed turbidity. After 1 hour under an unspecified stirring, the solution became clear, indicating miscibility, which probably meant total alkoxysilanes hydrolyzation with available silanol groups to react in the further condensation reaction. Although, the observed increase of viscosity of the solution also means that some condensation already occurred.
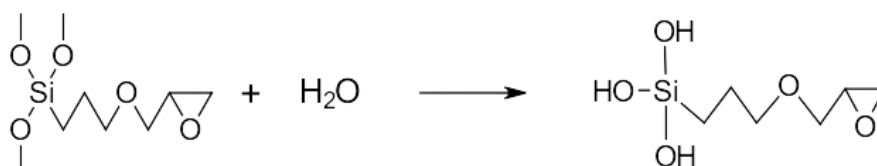
Figure 24 – Possible GPTMS hydrolysis reaction.

Figure 25 – Possible TEOS hydrolysis reaction.

4.1.2. W/O emulsion

SPAN 80 appliance in this specific emulsion is due to its HBL value of about 4, suitable for the continuous phase of W/O emulsions. The resultant emulsion had a milky appearance what proves that a successful W/O emulsion was made as in other typical emulsions of this kind. Moreover, the denoted change from opaque to translucent when the pre-hydrolysate's addition is made may indicate it works as a co-solvent due to the alcoholic species released during the hydrolysis. This reason could explain the certain instability observed by the water droplets' coalescence (Figure 26). It is important to note that the prepared emulsions were made in the same way, and their appearance was similar. Thus, a deep understanding of this matter is important, so further studies should be made regarding the emulsion's stabilization, in order to avoid droplets coalescence.

Apart from that, the formed microemulsion appears to be bi-continuous, and besides its great stability, it may not be the more appropriate for the intended purpose, seeming that the actual microemulsion is only formed after the silanol solution is added (Figure 26).

(i)   (ii)

Figure 26 – Representative emulsion's optical photomicrograph before (i) and after (ii) the pre-hydrolysate addition. Bar scale = 300 µm (SP33).

4.1.3. Formation of the MSs: stimulating condensation by pH

In this study, a specific temperature was fixed while the reaction was occurring, and small amounts of ammonia were added, to increase the pH of the reaction's medium, promoting condensation so particles could be formed. The synthesis was carried out for 65, 75, 80, and 85°C.

The first assumption to be taken was in terms of the size of the particles. As shown in Figure 27, the higher the reaction's temperature, the bigger the particles' size.

| (i) | (ii) | (iii) | (iv) |
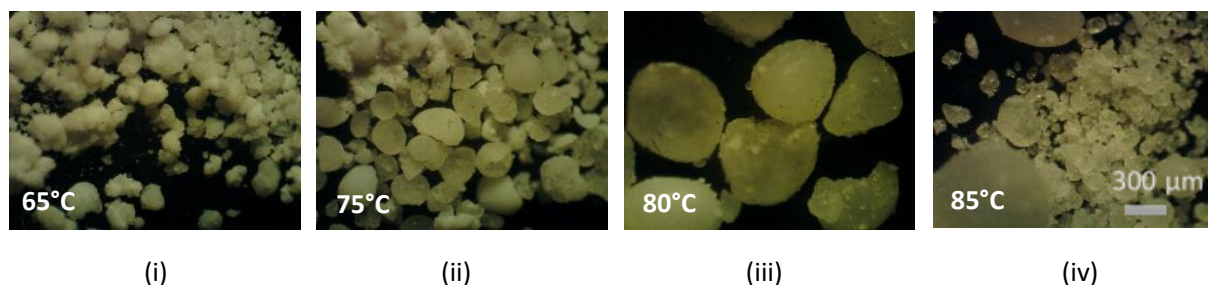
Figure 27 – Optical microscopy photographs of the syntheses results according to the fixed temperatures (i-iv). Bar scale = 300 µm.

In Figure 28 (SP13 (ii) and SP9-SP11 (i)), the reaction's evolution seems to create a siloxane-in-water-in-oil system. It may probably be explained by the loss of polarity of the previous hydrolysed precursors. After adding the pre-hydrolysate to the W/O emulsion, the silanes with silanol groups spontaneously diffuse to the droplets' interior due to polarity stabilization. Water is the highly polar solvent composing the droplets of the W/O emulsion, making this diffusion possible to occur through the surfactant. Throughout the condensation, the Si-OH moieties react, gradually losing polarity due to water elimination, thus losing the OH groups. The formation of water brings more quantity of it to the droplets system, which may have led to increased surface tension between the droplets, and to decrease that, they agglomerate, creating a gel(siloxane)-in-water-in-oil microemulsion.

The supposedly gel/W/O emulsion is created earlier by increasing the fixed temperature, which evidences the temperature's influence on the condensation's rate.

Besides promoting the polymerization reactions, the addition of ammonia also seems to be promoting the agglomeration of the content inside the "bigger droplets", creating large particles with apparently some porosity due to its opaque feature.

Figure 28 also shows that as the amount of ammonia in the reaction increases, the pH of the reaction medium does not change (it would be expected to increase). This indicates that the hydroxide ions in solution are being consumed, probably by GPTMS organic moieties.
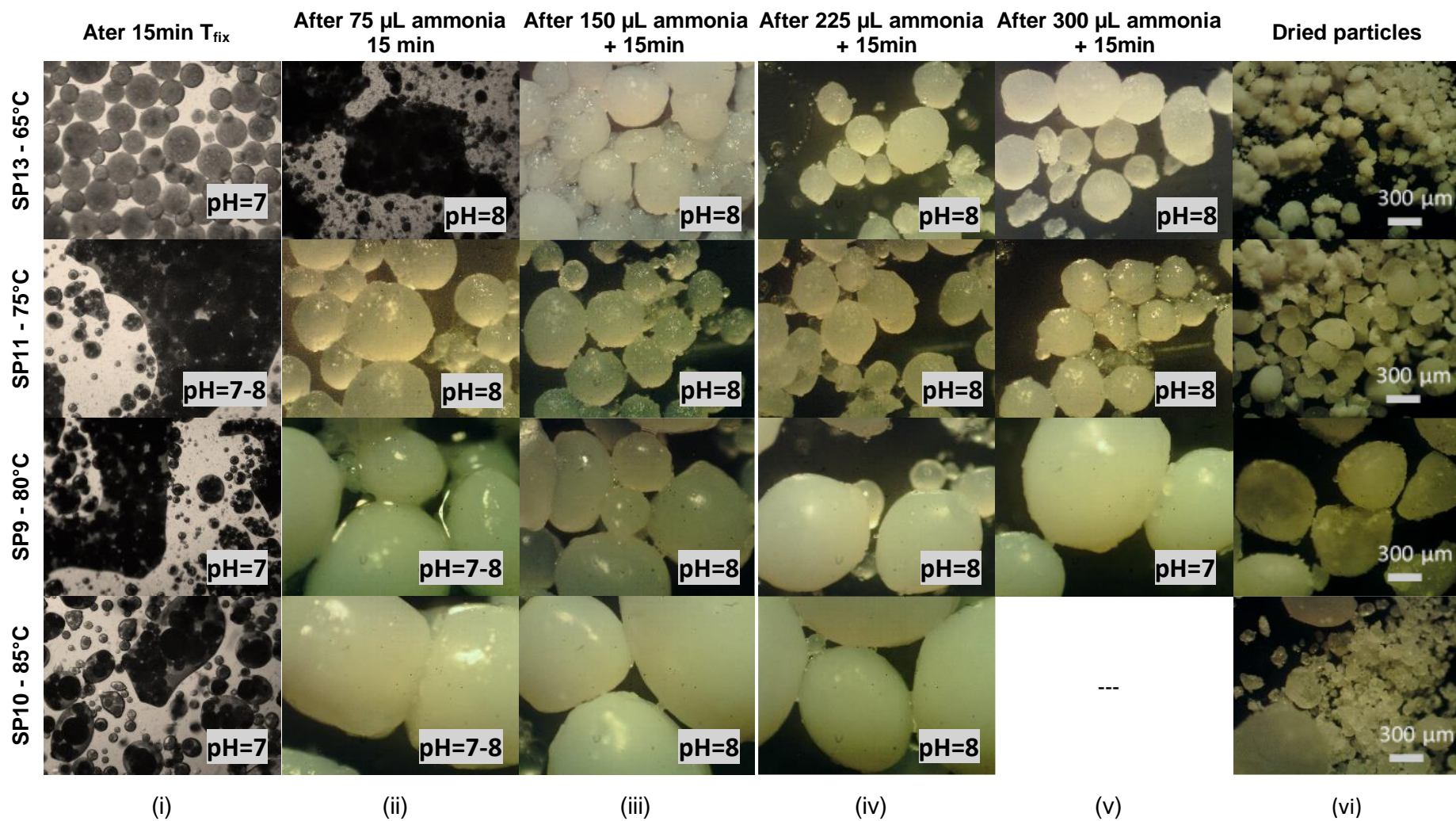
Figure 28 – MSs' formation by stimulating condensation through pH: evolution of the reaction's medium as ammonia was added (i-vi). Bar scale = 300 µm.

4.1.4. Formation of the MSs: stimulating condensation by temperature

This study intended to reproduce the successful silica MSs synthesis developed in the work before this dissertation. The photomicrograph obtained for those MSs is presented in Figure 29.
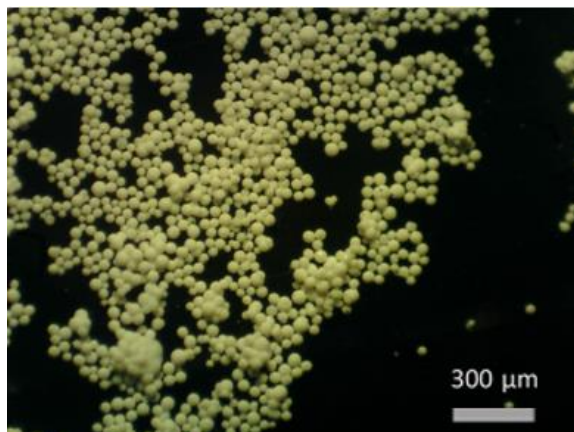
Figure 29 – MSs' optical photomicrograph obtained in the SE12 synthesis at previous studies to this dissertation. Bar scale = 300 μm.

The protocol followed for the attainment of those MSs (introduced in Chapter 3.2) was repeated several times what allowed to conclude that such a procedure was not easily reproducible. Although, as shown in Figure 30 and Figure 31, for the SP19 and SP26 syntheses, it was possible to achieve MPs but not in perfect spherical shape as those trying to be reproduced (Figure 29). The optical photomicrographs for the remained performed syntheses can be accessed in Appendix A.

The surface's morphology seems identical for both presented particles, but their size is in the range of 50-225 μm and 35-100 μm for SP19 and SP26, respectively. The procedure was indeed the same, and in a closed system, so the external conditions should not influence the results, and besides, the temperature room was similar in both cases. For what is concerned, the only parameters that could justify their difference in sizes were the addition time (or rate) of the pre-hydrolysate to the W/O emulsion, the degree of polymerization of the pre-hydrolysate, and the initial temperature under which the condensation takes place. At this stage of the carried studies, such addition was done with a dropping funnel as support, making it difficult to control the addition's rate, always causing different addition times. The exact influence of this parameter in the polymerization reaction is unknown; a further attempt to control it was made within this study.

Both SP19 and SP26 were considered successful experiments due to the intended range size and presented interconnected macroporosity (Figure 32). This latter feature is characteristic of the phase separation by spinodal decomposition. Such separation was induced by polymerization-condensation reactions leading to "chemical quenching", i.e., the changing of location in the phase diagram of the critical point which, as referred to in the theoretical overview, is dependent on the polymerization degree (number of statistical segments) which increases with the course of condensation reactions.

	Emulsion	After 1 hr at 65˚C	After 10 min a 70˚C	Após 15 min a 75˚C	Após 1 hr a 80˚C	Dried particles
SP19						300 µm
SP26						300 µm
	(i)	(ii)	(iii)	(iv)	(v)	(vi)
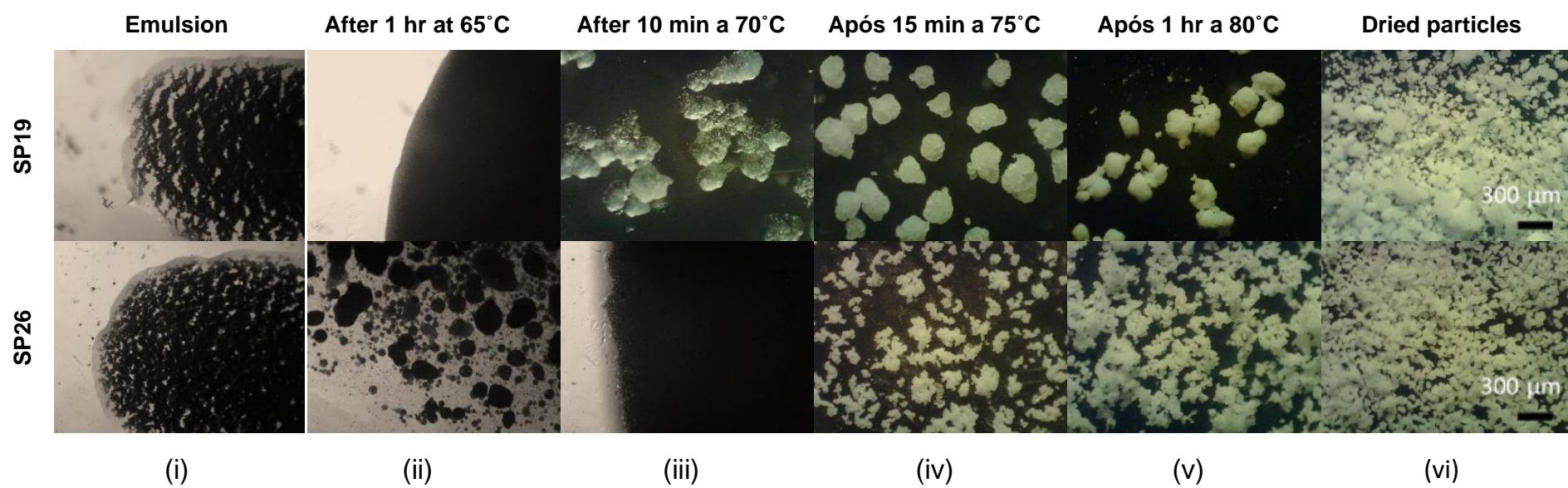
Figure 30 - Optical microscopy photographs of the reaction's medium according to the temperature and time described in Table 4 of the SP19 and SP26 synthesis (i-vi). Bar scale = 300 µm.
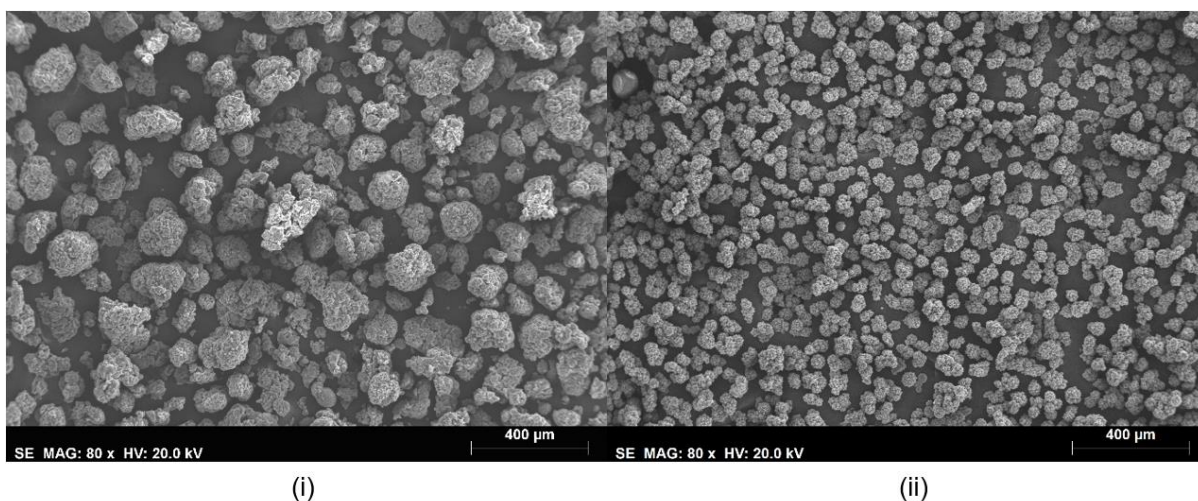
Figure 31 - SEM photomicrographs of the produced MSs. (i) SP19 MSs; (ii) SP26 MSs. (x80, bar scale = 400 μm).
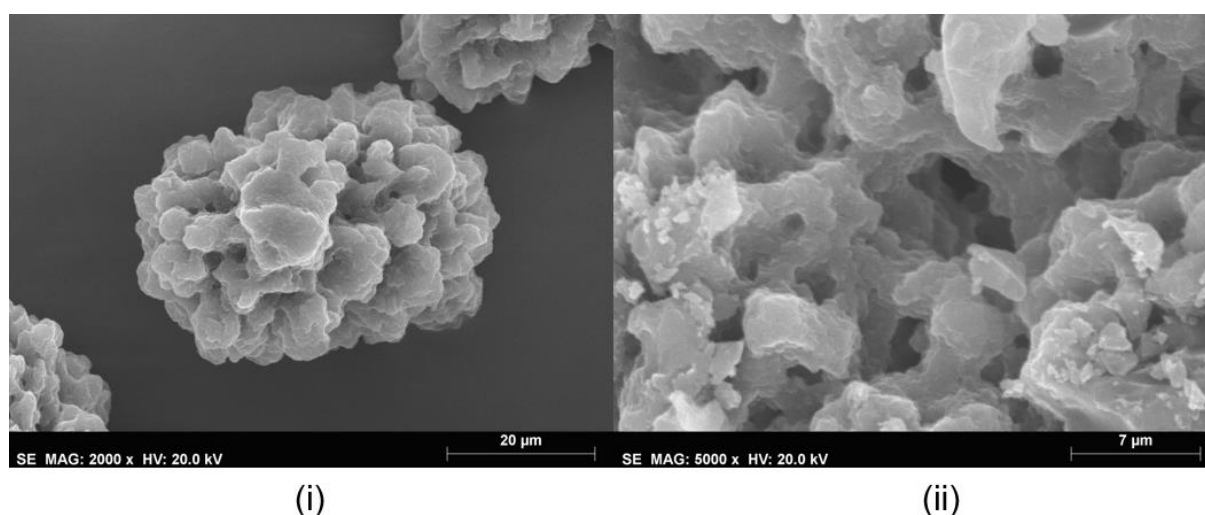
Figure 32 - SEM photomicrographs of the surface (i) and internal structure (ii) of the SP26 MSs.

((i): x2000, bar scale = 20 μm; (ii): x5000, bar scale = 7 μm)

For the following results, SP26 synthesis will be presented for comparison, since it shows a homogeneous size distribution within the intended range, becoming the one to be reproduced.

60% of the pre-hydrolysate solution

The influence of reducing 40% of the pre-hydrolysate mass quantity added to the emulsion was studied. The results are presented in Figure 33.

The addition of a lower quantity of pre-hydrolysate solution is found to result in less stabilization of the W/O emulsion. If there is less quantity of pre-hydrolysed species for the same volume of the reaction medium, the distribution of those for the various droplets is more extensive, i.e., there is less concentration of those within the droplets, resulting in limited water phase droplets coalescence.
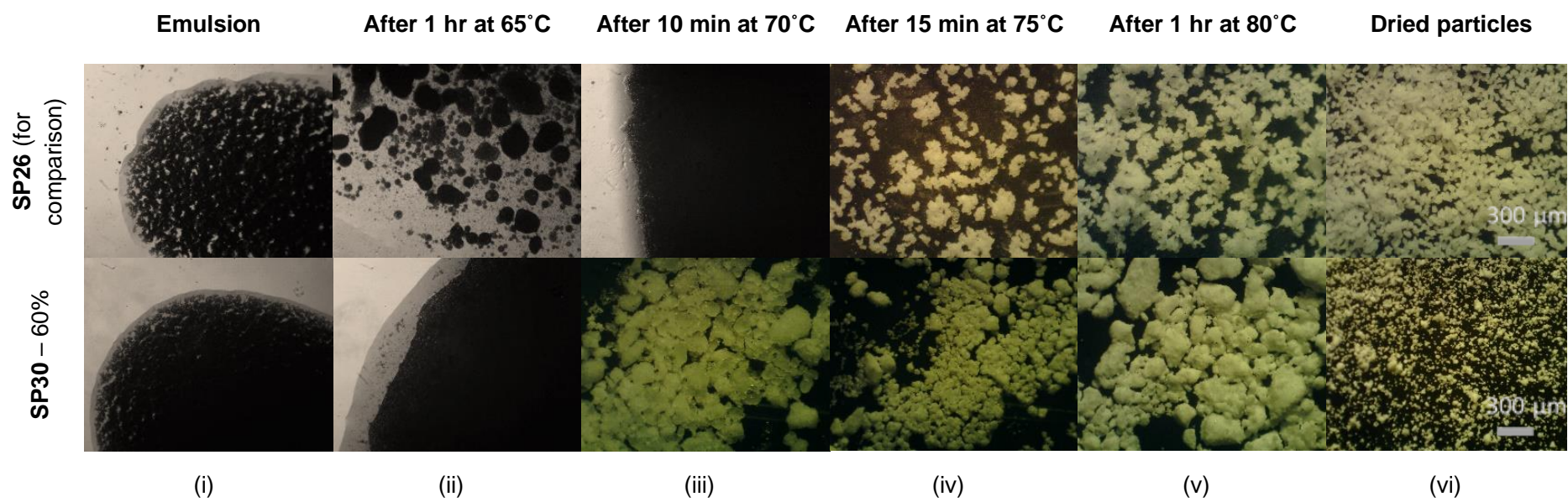
Figure 33 - MSs' formation by stimulating condensation through temperature with 60% of the pre-hydrolysate mass studied before: evolution of the reaction's medium according to the temperature and time described in Table 4 *for SP26 and SP30 syntheses (i-vi). Bar scale = 300 μm.*

Figure 33 (SP30 (iv) and (v)) shows the formation of irregular particles that, after drying, disaggregate (Figure 33 (vi)), and Figure 34 confirms the presence of those particles that were previously aggregated.
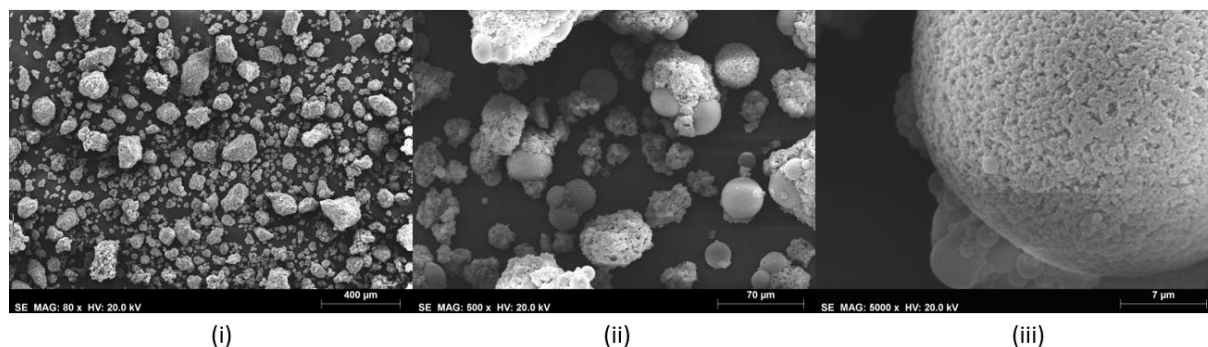
Figure 34 - SEM photomicrographs of SP30. ((i): x80, bar scale = 400 μm; (ii): x500, bar scale = 70 μm; (iii): x5000, bar scale = 7 μm)

Regarding the droplet system, the induced phase separation by chemical cooling (specifically by the condensation reaction) is easier to be accomplished when the solution's position in the phase diagram (siloxane concentration) is around the critical composition. Inside the droplets, water is the solvent for the hydrolysed species, so polymerization only occurs for the silica monomers what means the phase diagram is asymmetric (the system is constituted with species with different polymerization degrees). Since there is a lower concentration of hydrolysate, the solution's position in the phase diagram is closer to the water-rich side than in the previous syntheses. This may indicate that in SP30, the monomers' polymerization induces the development of a co-continuous structure that freezes late, resulting in fragmentation of the domains and then spheroidization, thus an interconnected structure of particles aggregates.

This separation has some similarities to the FA-system of Kaji et al. (1993) [21], but instead, it happens within the droplets. As presented in Figure 13, the co-continuous structure formed (referred to the spinodal decomposition) is a transient structure that grows while maintaining the connectivity during a limited time and later turns into a fragmented structure due to the minimization of the energetically unfavourable interfaces forming aggregates of particles probably just like happens in SP30.

On the other hand, another possible reason for the obtained MSs, in SP30, is the lower degree of emulsion destabilization that leads to the formation of small diameter porous MSs. The heterogeneity observed in this sample (perfect porous MSs surrounded by porous fragmented material) probably derives from the agglomeration of the content inside the "bigger droplets".

Amount of SPAN80 in the emulsion

The surfactant influence in the reaction was studied for 2, 4, and 6 g of it. Figure 35 suggests that smaller particles can be formed with a higher amount of surfactant, which has been already reported before. If there is a larger surfactant concentration for the same emulsion, more and smaller droplets will be created since there is an increased number of surfactant molecules. Thus, smaller micro-reactors will be available for condensation, leading to smaller particles' formation. Figure 36 also corroborates this

latter statement by showing bigger droplets for less surfactant's content (this before gelation, which is pointed by dense and darker emulsions). It can additionally be seen that the lesser the amount of SPAN 80, then later the gelation occurs. What is explained for the larger volume available to house the hydrolysate, allowing more polymerizable material inside it; therefore, more time is required until gelation.

(i)   (ii)   (iii)
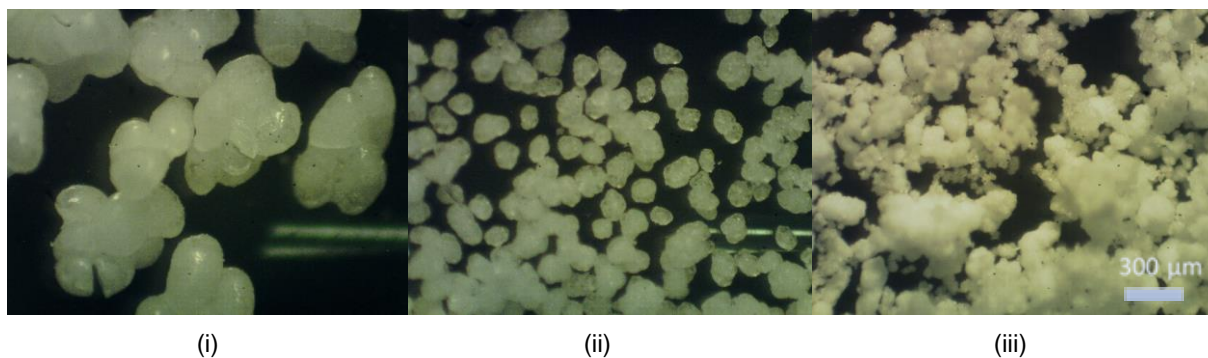
Figure 35 – Optical photomicrographs of the dried particles resulted from the syntheses SP21 (i), SP22 (ii), SP20 (iii) with 2, 4, and 6 g of SPAN 80, respectively.
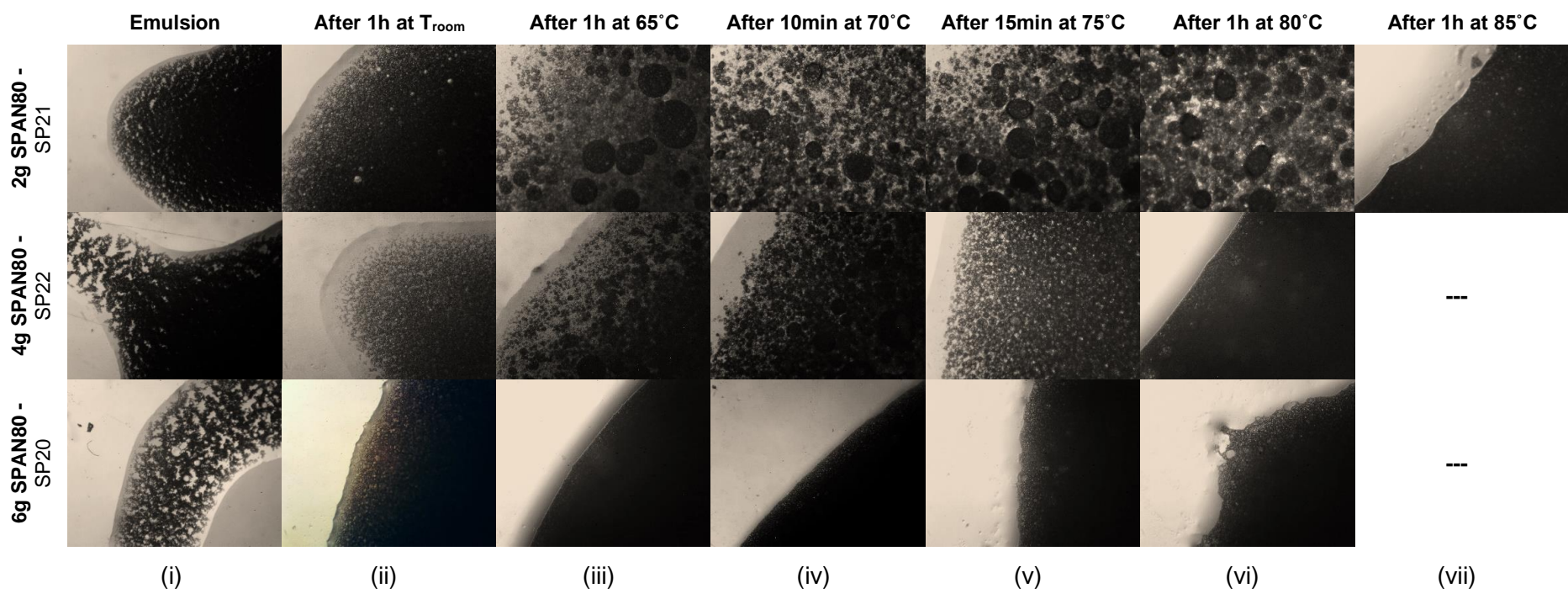
Figure 36 - Emulsion's evolution when condensation is stimulated by temperature according to the temperature and time described in Table 4 for different amounts of surfactant for SP20-SP22 syntheses (i-vi).

Controlled addition rate of the pre-hydrolysate to the emulsion

With the support of a peristaltic pump, it was possible to control the hydrolysate's addition to the emulsion template. For most experiences within this study, 30 minutes was established since that was the time performed in SP26 synthesis. Some other times were tested; therefore, the results did not achieve the intended, and their influence throughout the reaction was quite inconclusive.

It was possible to produce MSs with a controlled addition time of 30 minutes within the wanted range size for SP40 and SP41 syntheses (about 40-100 µm for SP40 and 60-110 µm in SP41), as seen in Figure 37.
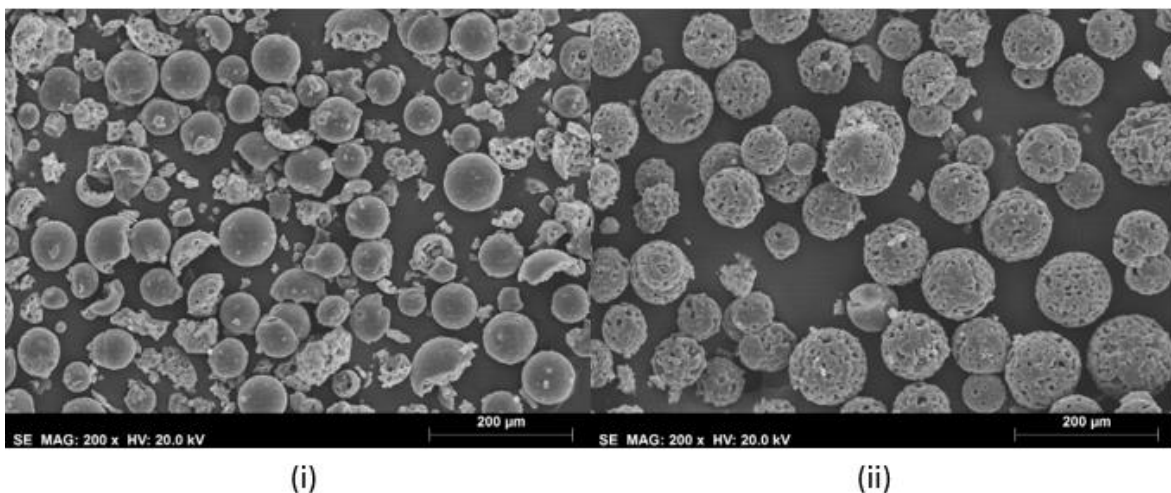
Figure 37 - SEM photomicrographs of the MSs produced by controlling the addition time (30 minutes) (x200, bar scale = 200 µm). (i) SP40 MSs; (ii) SP41 MSs.

It is notable a difference in the structures of both MSs. At the first look, SP40 MSs (Figure 37 and Figure 38 (i)) seem to be dense and nonporous, while SP41 MSs (Figure 37 and Figure 38(ii)) appear to have the intended interconnected macroporosity. Various reasons may justify this difference.
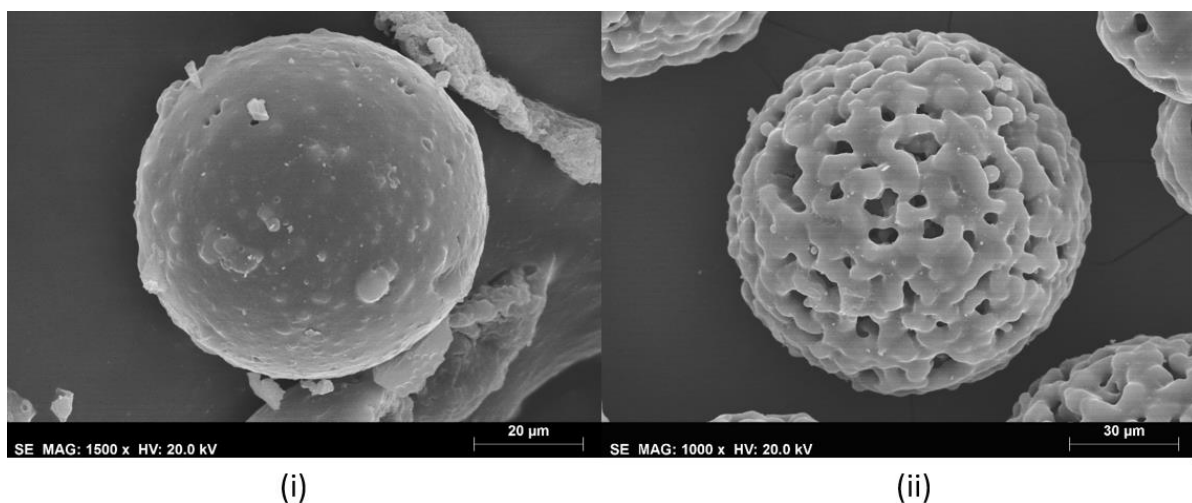
Figure 38 - SEM photomicrographs of the surface of the SP40 (i) and SP41 (ii) MSs. ((i): x1500, bar scale = 20 µm; (ii): x1000, bar scale = 30 µm)

Firstly, the water content in SP40 was 40 g instead of 45 g. This slight difference could have moved the droplet's system (in the phase diagram) near to the siloxane-rich side, leading to a C-type structure like in Figure 13. This morphology results from gradual gelation from the bottom of the precipitated silica-rich phase, which also means it late freezes, creating a "two-phase" structure [1,2].

Figure 39 (i) proves the existence of that spinodal decomposition "two-phase" separation of SP40, where the spheric pores are assumed to be the spaces where the water solvent was entrapped within the silica-rich phase from where it could not escape during coacervation. Also, Figure 39 (ii) shows the interconnected macropores of the SP41 MSs and resorting to Figure 13 again, it looks like a spinodal decomposition closer to the critical composition, probably with early freezing due to the formed continuous thinner structure.

SE MAG: 3000 x HV: 20.0 kV   10 µm   SE MAG: 3000 x HV: 20.0 kV   10 µm

(i)   (ii)
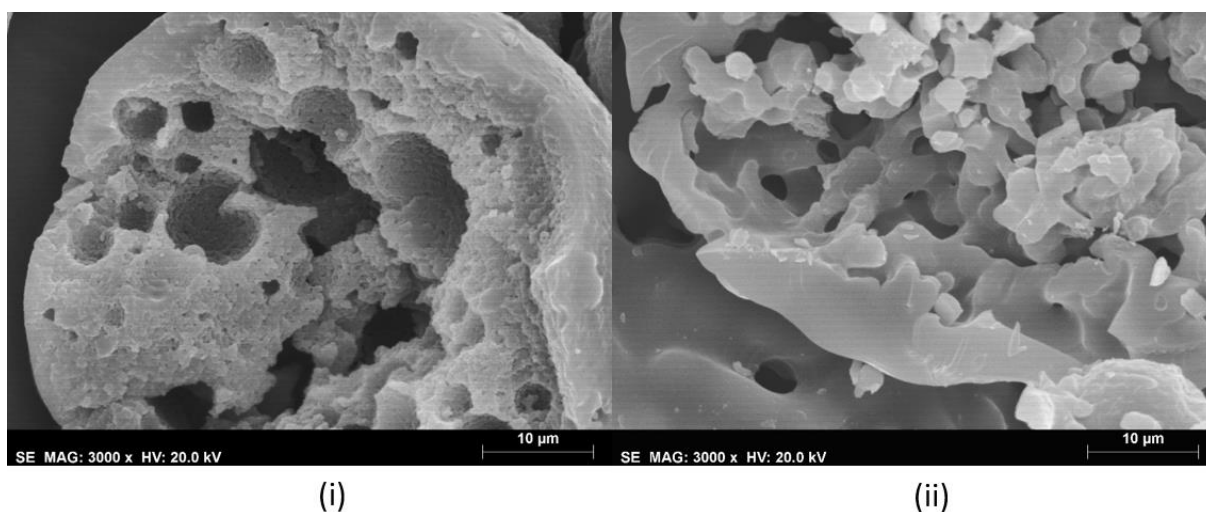
Figure 39 - SEM photomicrographs of the internal structure of SP40 (i) and SP41 (ii) MSs. (x3000, bar scale = 10 µm)

Other parameters that could explain the presented differences and the course of the reaction (Figure 40) – either in these or in the other syntheses – are the not controlled initial temperature of condensation and the viscosity of the pre-hydrolysate, which are parameters that may influence the chemical quenching course for structure formation (either late or early freezing).

	Emulsion	After 1 hr at 65˚C	After 10 min at 70˚C	After 15 min at 75˚C	After 1 hr at 80˚C	After 1 hr at 85˚C	Dried particles
SP26						---	
SP40							
SP41							
	(i)	(ii)	(iii)	(iv)	(v)	(vi)	(vii)

Figure 40 - MSs' formation by stimulating condensation through temperature with a controlled pre-hydrolysate addition rate: evolution of the reaction's medium according to the temperature and time described in Table 4 for SP26, SP40 and SP41 syntheses (i-vii). Bar scale = 300 µm.

For a large part of the experiments, the silanes hydrolysates' viscosity were assessed and are presented in Chapter 4.2.

Another probable influence lies in the fact that it was necessary to hydrolyse a more significant amount of silanes for viscosity measurements, but this was done by maintaining 1 hour of pre-hydrolysis, which led to a different degree of polymerization of alkoxysilanes; perhaps lower.

The cluster of gelled particles seen in stages (iv) of SP40 and (v) of SP41 was verified for many other syntheses carried out, as shown in Figure 40 and Appendix A. When this happened, these particles usually agglomerated, giving rise to much larger particles. So for SP40 and SP41, adding acetone to the reaction medium was an attempt to separate them. Since acetone is a polar solvent, having an affinity with water but not with the gel, it was believed it could allow this separation. However, as can be seen in t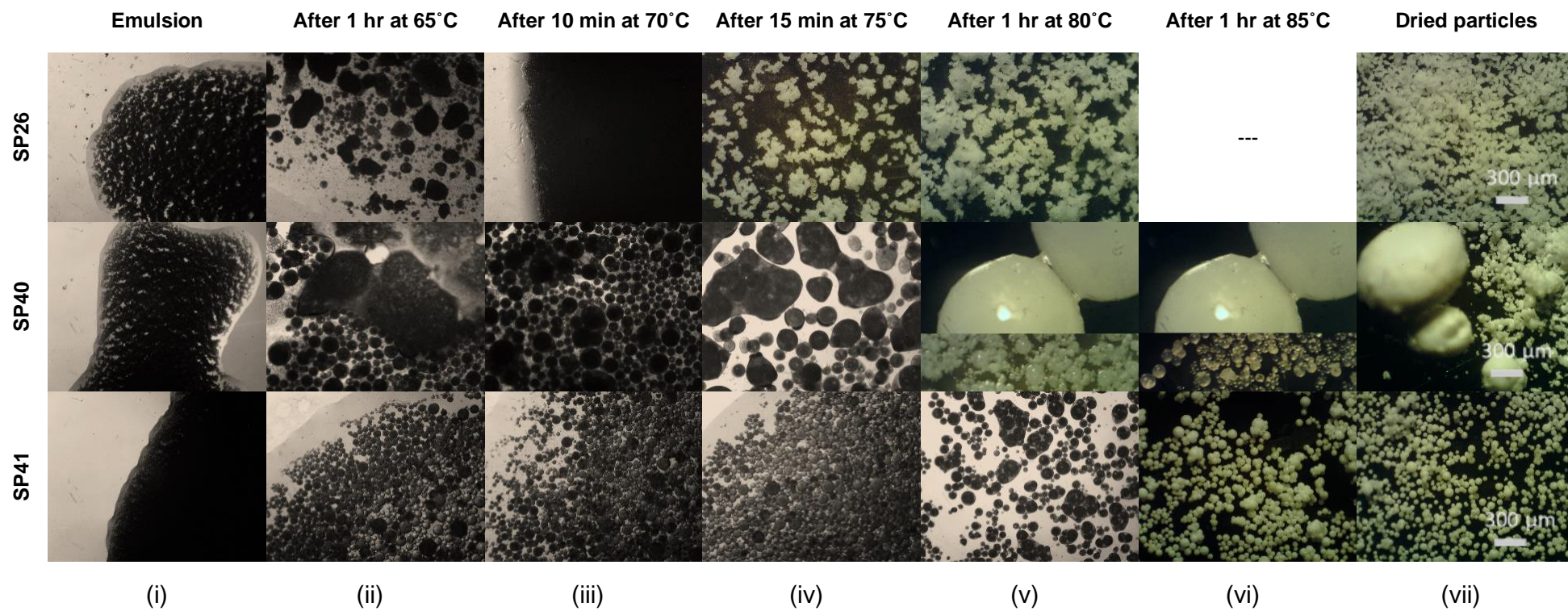he following stages, the effect was not what was intended. In SP40, clusters of different sizes are seen, which thus originated particles of different sizes. In SP41, clusters of fewer particles are presented, most of which are already isolated in a water enclosure. Thus, acetone did not establish the necessary repulsion forces between the particles to avoid their aggregation.

4.2. The viscosity of the pre-hydrolysed solution

The viscosity of the pre-hydrolysate is related to the degree of polymerization of the alkoxysilanes employed. It is influenced by the pH of the solution, temperature and the duration time of the pre-hydrolysis. As been stated before, the pH has a significant influence on the hydrolysis and condensation relative rates. The pre-hydrolysis is performed in acidic conditions to minimize condensation and allow hydrolysis completion. The more time for it to happen, along with the completed hydrolysed silanes, the more condensation reactions will occur, so more viscous will be the solution.

The hydrolysates' viscosity was measured when pre-hydrolysis takes 1 hour (Table 5).

Table 5 – pH and viscosity of the silanes pre-hydrolysate and room temperature for the syntheses that comprised a pre-hydrolysis time of 1 hour.

Sample acronym	pH	T_{room} (ºC)	Viscosity (cP)
SP35	5	16,8	8,36
SP36	5	17,5	8,34
SP34	5	17,6	8,26
SP33	5	18,1	8,38
SP43	5	23,6	8,36
SP40	6	23,4	8,54
SP41	6	22,1	9,20
SP42	6	24,6	9,08

It seems the hydrolysate viscosity may influence the particles' size, more precisely it indicates the presence of more siloxane oligomers which are apolar groups that compose the spheres inside the

"bigger droplets". Thus, those spheres do not have affinity with the water around them, so to stabilization, they agglomerate. Hence, the viscosity can also be seen as a measure that indicates if the gelled phase inside the "big droplets" is more likely to agglomerate or not (Appendix B). Also, room temperature may influence to accomplish higher values of viscosity, as Table 5 suggests. For the higher value of viscosity achieved (9,20 cP) in SP41, it was possible to produce defined MSs with macropores, so experiences were made with an attempt of increasing this parameter by performing 24-hour hydrolysis. The results are shown in Table 6.

Table 6 – pH and viscosity of the silanes pre-hydrolysate for the syntheses that comprised a pre-hydrolysis time of 24 hours.

Sample acronym	pH	Viscosity (cP)
SP52	6	10,20
SP54	6	10,90
SP55	6	10,50

The 24-hour hydrolysis allowed values of viscosity always greater than 10 cP. However, for those experiments, no particles could be produced. As seen in Figure 41, the emerge of particles never happened, like in the previously performed syntheses (Appendix B), and by reaching 85 ºC, the droplets seem to be shattered, and their content spread throughout the continuous phase of the emulsion. No explanations were found for this occurrence.

The viscosity appeared to be challenging to control since it was not possible to regulate the stirring rate when hydrolysis was performed because it was limited to the available laboratory materials.
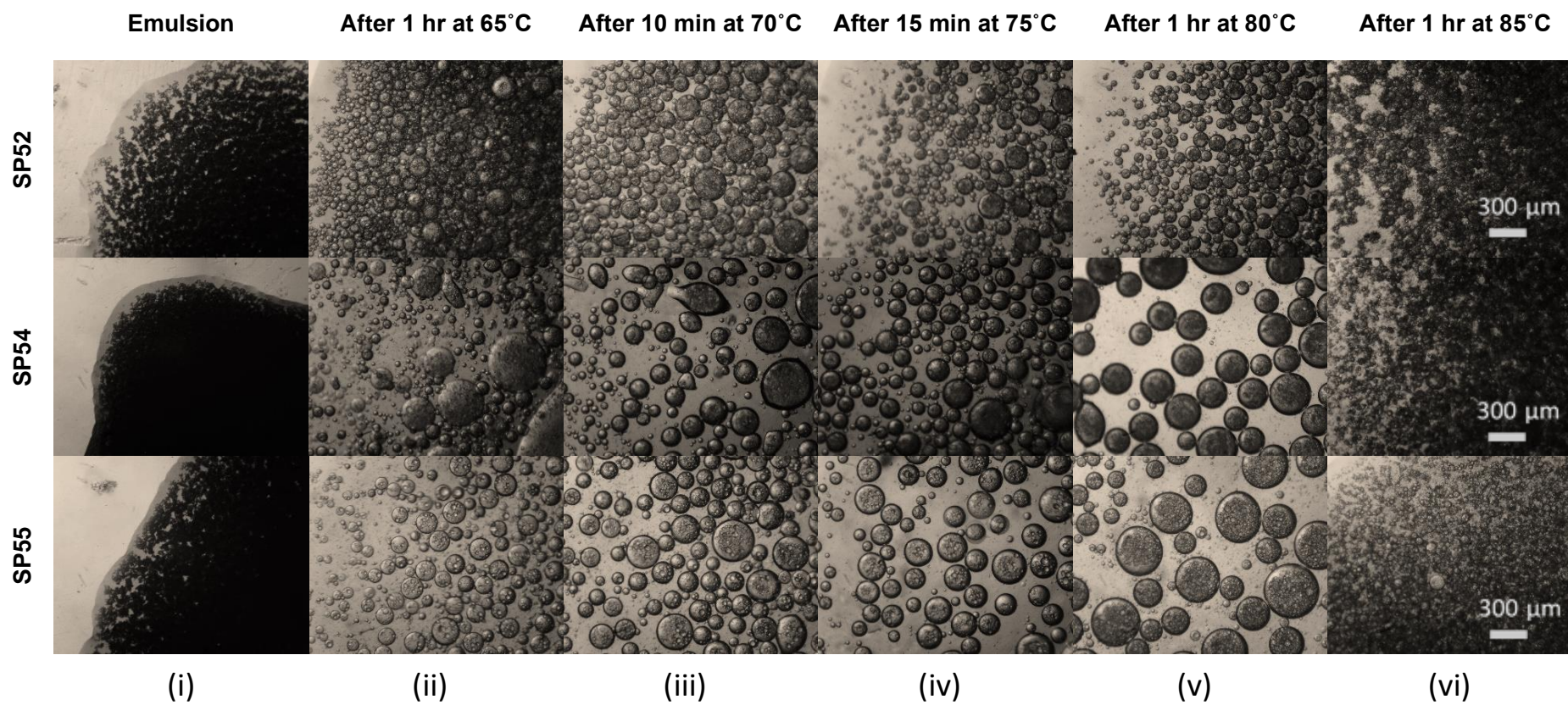
Figure 41 - Evolution of the reaction's medium according to the temperature and time described in Table 4 for SP52, SP54, and SP55 syntheses – 24-hour syntheses (i-vi). Bar scale = 300 µm

4.3. TiO₂ immobilization into the MSs

The nanoparticles TiO$_2$ (P25) were impregnated in the produced SP26 MSs. The following characterization will confirm the suitability of the MSs with interconnected macroporosity for immobilization of different compounds.

Figure 42 comprises the SEM photomicrographs previously to the immobilization ((i)-(ii)) and after the immobilization ((iii)-(iv)) with the NPs. Comparing them, some "new" material deposited in the surface of the particle that has been coated with NPs can be identified, thus confirming the existence of NPs and consequently the success of the entrapment process.
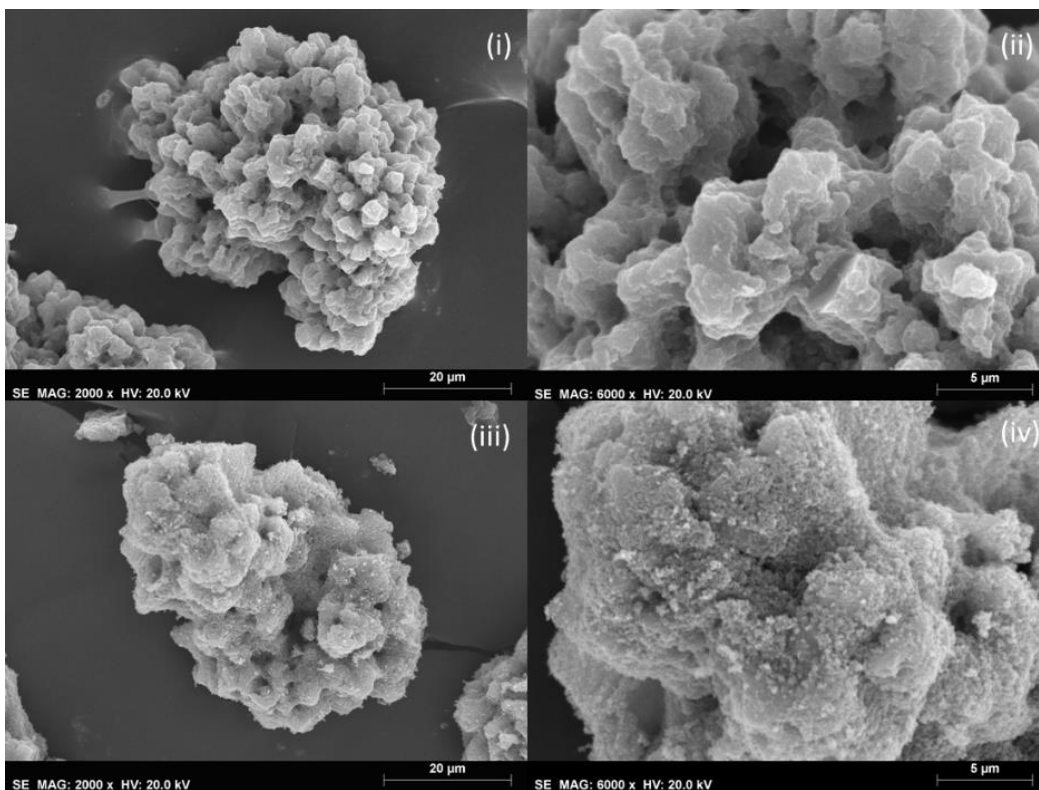
Figure 42 - SEM photomicrographs of the SP26 MSs before (i)-(ii) and after (iii)-(iv) the impregnation of TiO$_2$ NPs. ((i) and (iii): x2000, bar scale = 20 µm; (ii) and (iv): x6000, bar scale = 5 µm)

The EDX images are presented in Figure 43, and it is a useful analysis for confirmation of the presence of TiO$_2$ NPs within the MSs since it is a qualitative analysis of the existing chemical elements, i. e., by identifying the presence of the elements that compose the NPs, namely titanium, EDX gives the information of its existence or not, but do not quantifies the amount of it. The EDS graphs can be accessed in Appendix C for noticing chemical elements relative to the counts in a sample's fraction.

Analyzing Figure 43, titanium and silicon, are the elements detected. The latter confirms the scaffold is made of silica, and the former confirms the presence of the NPs within these scaffolds (Figure 43 (ii), (iii) and (iv)). Its distribution seems relatively homogenous but with slight densification on the scaffold's exterior surface. These results corroborate what was observed in the SEM photomicrographs.
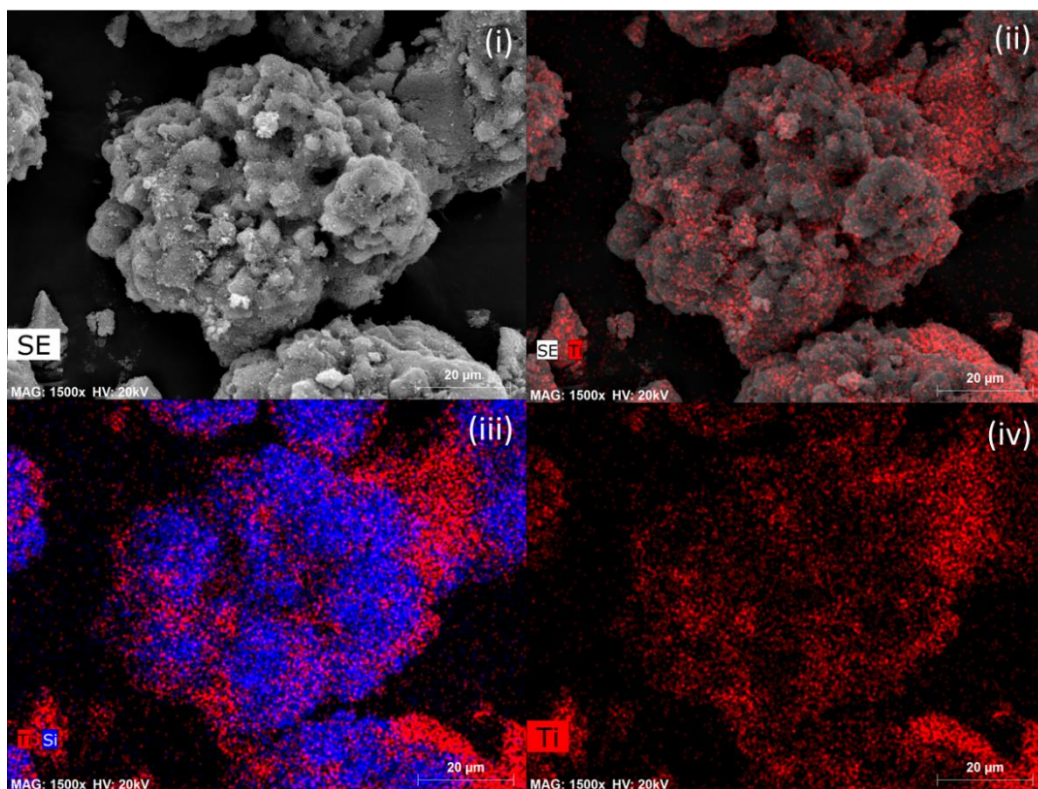
Figure 43 - EDX images of the SP26 MSs after the impregnation with TiO$_2$ NPSs. Detection of titanium in (ii), (iii), and (iv). Detection of silicon in (iii). (x1500, bar scale = 20 μm)

FTIR-ATR had the purpose of characterizing the MSs chemical structure, i.e., to give the composition of the matrix and consequently the presence of the TiO$_2$ NPs, before and after heat treatment and immobilization of the NPs.

Figure 44 shows the spectra of the SP26 MSs and TiO$_2$ NPs. The spectrum for TiO$_2$ displays two peaks at 3200-3500 and 1610 cm^{-1} (denoted by the asterisks (*)) assigned to the stretching vibrations of surface hydroxyl groups and bending vibration of molecular water absorbed, respectively, and a strong absorption band at 500-600 cm^{-1} ascribed to Ti-O-Ti bonds stretching. The SP26 MSs present the typical peaks of silica-based materials at 1030 cm^{-1} with a shoulder at 1090 cm^{-1} corresponding to Si-O-Si asymmetric stretching. The peaks 908 and 850 cm^{-1} are ascribed to the stretching of C-O and C-O-C relative to epoxy groups confirming the organic contribution of GPTMS to the MSs, and its hybrid character. At 3200-3500 cm^{-1}, there is also a peak, like in TiO$_2$ NPs, representing the -OH stretching [1,74].

After heat treatment of the MSs at 900 ºC, the FTIR-ATR spectrum relative to the MSs turned out different which is typical of inorganic silica materials. The peaks relative to C-O, C-O-C, and -OH stretching disappeared. It is clear at ca. 800 cm^{-1} the presence of a peak that belongs to Si-O-Si symmetric stretching, as well as a peak at ca. 1090 cm^{-1} with a shoulder at 1200 cm^{-1}, ascribed for the Si-O-Si asymmetric stretching (transversal and longitudinal mode, respectively) [1,2]. These results and the ones for the MSs with TiO$_2$ entrapped can be accessed in Figure 45. The term SP26-HT denotes the SP26 MSs heat-treated and SP26-HT-I the MSs heat treated with NPs immobilized. SP26-HT-I does

not present any band alteration, appearing to be a superposition of the spectra of TiO_2 and MSs. Although, the intensity of absorption bands corresponding to Si-O-Si decreased, confirming the presence of TiO_2 that coated the MSs.
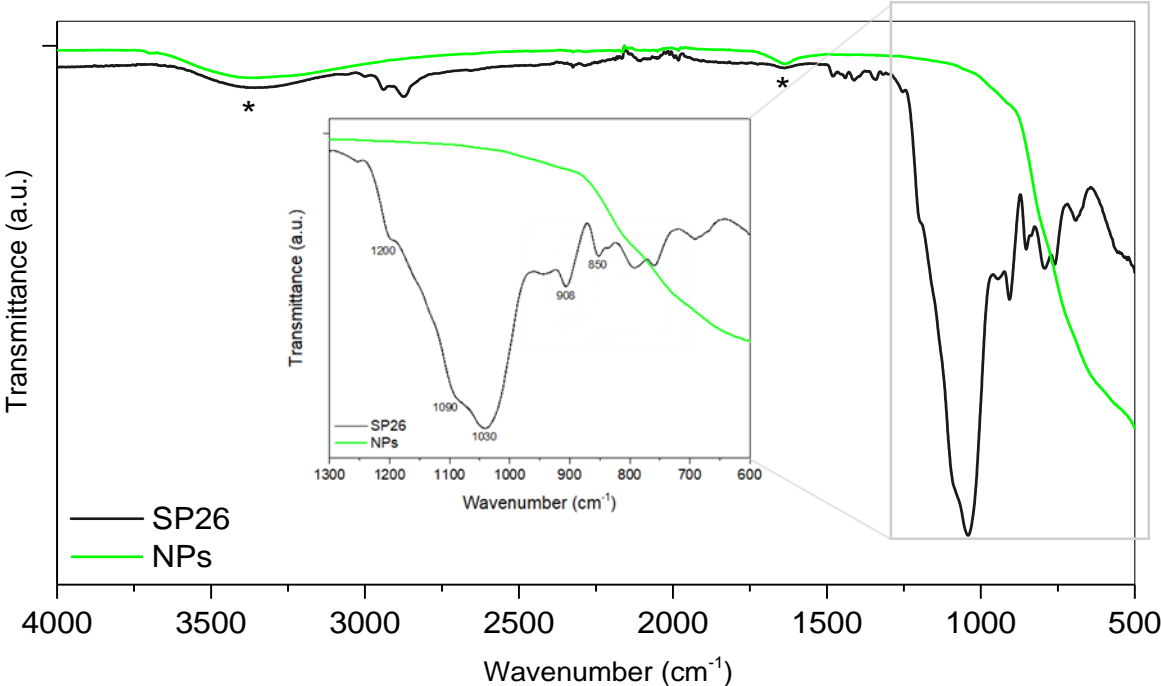
Figure 44 - Normalized FTIR-ATR spectra obtained from MSs before heat treatment of 900 ºC (SP26: black line) and from TiO_2 NPs (NPs: green line).
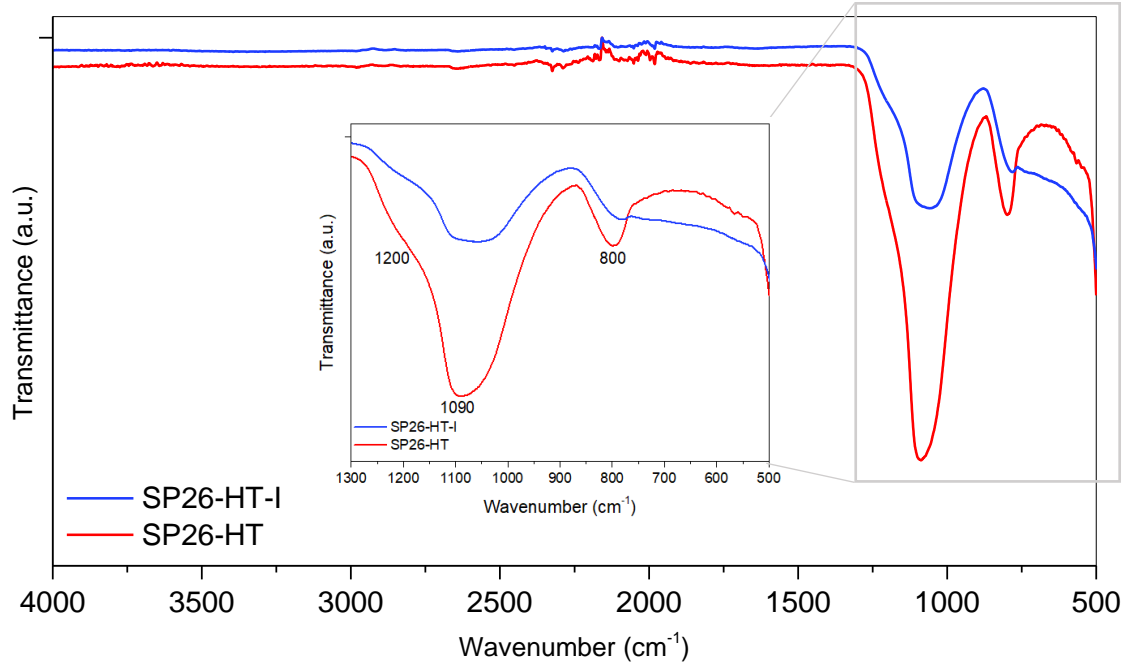
Figure 45 - Normalized FTIR-ATR spectra obtained from MSs before (SP26-HT: red line) and after the impregnation with NPs (SP26-HT-I: blue line).

By a spectra magnification and normalization between 1500 and 700 cm^{-1} (region referred to the Si-O-Si peak) (Figure 46), it is shown a strong contribution from the large band at low wavenumbers related to Ti-O-Ti bonds stretching. After the impregnation, the heat treatment at 500 ºC may have led to the establishment of covalent bonds between the NPs and the MSs through condensation reactions between Si-OH and Ti-OH moieties, originating Si-O-Ti bonds (SiO^{-}), which are typically presented at ca. 945 cm^{-1}. However, this region of the spectrum is also affected by Ti-O-Ti band contribution, so it is not possible to confirm the presence of Si-O-Ti bands by this characterization technique.
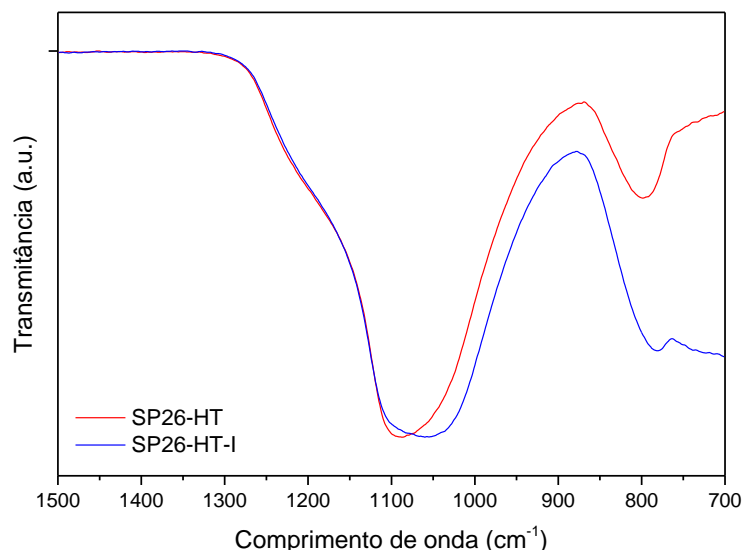
Figure 46 – Spectra magnification and normalization of the Si-O-Si peak region (between 1500 and 700 cm^{-1}) obtained from MSs before (SP26-HT: red line) and after the impregnation with NPs (SP26-HT-I: blue line).

The thermogravimetric analysis reveals the presence of inorganic material, corroborating the FTIR results and, therefore, does not show weight decreasing, so it was impossible to estimate the loading of TiO_2 NPs in the MSs (Appendix D). However, its relatively homogeneous distribution along the surface of the MSs is clearly shown at the SEM photomicrographs and the presence of TiO_2 is revealed by FTIR spectroscopy.

5. Conclusions and Future Perspective

The presented work regarded the production of porous microscaffolds, i.e., silica MSs with interconnected macroporosity, induced by polymerization reactions that led to a phase separation through spinodal decomposition within the droplets of a W/O microemulsion-template. Two main methods, pH and temperature stimulated condensation, were employed in order to enlighten the porous microscaffolds formation process and further optimize their production.

Spinodal decomposition has been well investigated, however, its focus has been mainly for monoliths. The practical synthesis of MSs through the sol-gel process combined with spinodal decomposition has been essentially a trial-and-error experiment so that a deep enlightening of the MSs formation process is required, and the present thesis represents a large step towards this need.

The successful porous hybrid MSs created involved TEOS and GPTMS as precursors of a "two-step" sol-gel process wherein a pre-hydrolysis was initially performed to increase the condensation reaction yield and to control it more easily. The pH stimulated condensation (by addition of ammonia) revealed the formation of larger MSs for increased fixed temperatures. It evidenced that either pH and temperature promote the condensation reactions, managing creation of clusters ("big droplets") of siloxane particles, thus, a siloxane-in-water-in-oil emulsion in which the ammonia addition eventually led to the agglomeration of those siloxane particles inside the "big droplets" and thus, forming large MSs. In the condensation stimulated by temperature experiments, an ascendant profile of temperatures was the driving force of polymerization. The optimal parameters were found to be via controlled addition rate of a pre-hydrolysate with a viscosity of 9.20 cP. It is believed this parameter has a considerable influence during the condensation since it relatively measures the degree of polymerization prior to condensation and, consequently, the water introduced in the further reaction medium. Furthermore, it drives the polarity of the pre-hydrolysate which influences phase separation phenomena, and the promptness for gelation and condensation reactions.

All the experiments were performed with the same proportion of initial components and speed stirring either for the emulsification (18000 rpm) and polymerization reaction (600 rpm). The varied parameters were (a) the mass quantity of surfactant (SPAN 80), leading to the conclusion that an increased amount of SPAN 80 allows the formation of smaller particles; (b) the amount of pre-hydrolysate to the same emulsion was tested when it was 60% of the mass that was being utilized what headed to large particles formed by clusters of smaller particles that disaggregated after drying, what may have been due to a dislocation of the solution's composition in the phase diagram; (c) the pre-hydrolysis time as an attempt to control viscosity suggested that may exist an optimal value for it, probably around 9.20 cP (to which MSs with the intended size and morphology were possible to be formed) but when is higher than 10 cP, no MSs could be produced for this exact system.

It is presumed that the clusters of gelled particles inside "big droplets" of water are one of the critical stages for the successful production of MSs with the desired spheroidization and size in the micron-range. It depends on repulsion forces that may exist between the gelled particles. It may be overcome by a better process' optimization such as optimization of the initial conditions or adding a solvent with

affinity with water and at the same time, a non-solvent for the gel matrix – perhaps a compound with amphiphilic structure instead of acetone, which was the solvent tried in the experiments.

The evaluation of the particles through SEM-EDS and FTIR-ATR confirmed the production of macroporous hybrid MSs, and the impregnation/immobilization of TiO_2 NPs was also accomplished.

For further studies, control of the pre-hydrolysate viscosity to ascertain the existence or not of an optimal value is crucial; the experiment of microemulsion preparation done directly from the silanol solution (pre-hydrolysate), i.e., with less or no water addition. This way, the water produced from the condensation reactions can be progressively evaluated in terms of its influence, and from there, it may be possible to create a more stable emulsion.

6. A Suggestion of a new photocatalytic reactor setup

The development of continuous-flow photocatalytic reactors is crucial for testing the scaffolds acting as photocatalysts for the decomposition of pollutants under solar illumination.

To optimize the solar radiation exposure area is important to develop a layer with impregnated MSs, allowing a continuous flow-through operation of water within their pores so that photocatalytic activity can be improved. For what is concerned, the only way to accomplish that without any other support, is by inserting the MSs in a thin "container" where they are packed within the perfect amount to let water flow not only through their interconnected macropores but also between them.

Lucchini et al. (2018) [74] presented a setup reactor for monolith photocatalysts with immobilized TiO_2 NPs as well. The monolith was fixed in a holder composed of two movable parts and a quartz window that allowed simulated solar radiation passage and incidence on the monolith.
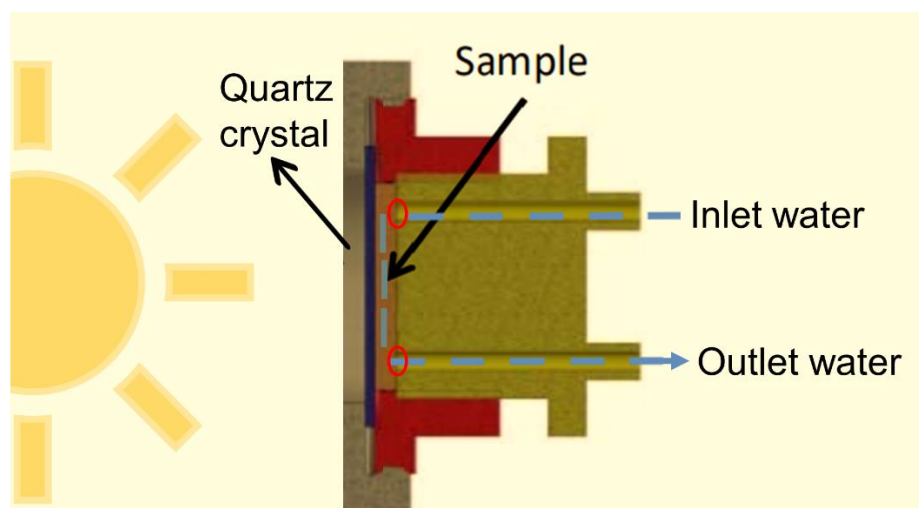
Figure 47 - Adapted reactor from [74] *as a suggestion of setup testing for loaded MSs.*

Based on the setup proposed by Lucchini et al. (2018) [74] the proposed here is to replace the sample's holder for the thin container where the in- and outlet of water will be incorporated with a filter suitable for MSs size, e.g., cotton, blocking the MSs to escape from the container inside and permitting the water solution to pass entirely through the MSs matrices (red circles in Figure 47).

Through this approach, a high contact between the active species and the contaminants is combined with a continuous flow operation. In addition, the MSs provide good physical fixation of the NPs, not releasing them during the process, enabling their reuse.

7. References

1. Vale, M.; Loureiro, M.V.; Ferreira, M.J.; Marques, A.C. Silica-Based Microspheres with Interconnected Macroporosity by Phase Separation. *Journal of Sol-Gel Science and Technology* **2020**, *95*, 746–759, doi:10.1007/s10971-020-05257-4.

2. Loureiro, M.V.; Vale, M.; de Schrijver, A.; Bordado, J.C.; Silva, E.; Marques, A.C. Hybrid Custom-Tailored Sol-Gel Derived Microscaffold for Biocides Immobilization. *Microporous and Mesoporous Materials* **2018**, *261*, 252–258, doi:10.1016/j.micromeso.2017.10.056.

3. Marques, A.C.L.; Loureiro, M. de J.V.; Geraldes, E.R.S.; Bordado, J.C.M. Custom-Tailored Sol-Gel Derived Matrixes for Chemical Immobilization 2018.

4. Alemán, J.; Chadwick, A. v.; He, J.; Hess, M.; Horie, K.; Jones, R.G.; Kratochvíl, P.; Meisel, I.; Mita, I.; Moad, G.; et al. Definitions of Terms Relating to the Structure and Processing of Sols, Gels, Networks, and Inorganic-Organic Hybrid Materials (IUPAC). *Pure and Applied Chemistry* **2007**, *79*, 1801–1829, doi:10.1351/pac200779101801.

5. Yang, Y.; Li, L.-H.; Li, Y.; Rooke, J.; Sanchez, C.; Su, B.-L.; Yang, X.-Y.; Chen, L.-H.; Rooke, J.C.; Ment Sanchez, C. Hierarchically Porous Materials: Synthesis Strategies and Structure Design. *Chem. Soc. Rev* **2017**, *46*, 481–558, doi:10.1039/C6CS00829Aï.

6. Assink, R.A.; Kay, B.D. Study of Sol-Gel Chemical Reaction Kinetics by NMR. *Annual Review of Materials Research* **1991**, *21*, 491–513.

7. *The Sol-Gel Handbook*; Levy, D., Zayat, M., Eds.; First Edition.; Wiley-VCH: Weinheim, 2015; Vol. 1; ISBN 9783527319916.

8. Innocenzi, P. *The Sol-to-Gel Transition*; Bhatia, S.K., Diebold, A., Hu, J., Krishnan, K.M., Narducci, D., Sinha Ray, S., Wilde, G., Eds.; Second Edition.; Springer Nature Switzerland AG: Gewerbestrasse, 2016; ISBN 978-3-030-20030-5.

9. Ghosh, S.K. Functional Coatings and Microencapsulation: A General Perspective. In *Functional coatings: by Polymer Microencapsulation*; Ghosh, S.K., Ed.; Wiley-VCH: Weinheim, 2006; pp. 1–28 ISBN 352731296X.

10. Ciriminna, R.; Sciortino, M.; Alonzo, G.; de Schrijver, A.; Pagliaro, M. From Molecules to Systems: Sol-Gel Microencapsulation in Silica-Based Materials. *Chemical Reviews* **2011**, *111*, 765–789, doi:10.1021/cr100161x.

11. Schramm, L.L. *Emulsions, Foams and Suspensions: Fundamentals and Applications*; Schramm, L.L., Ed.; Second Edition.; Wiley-VCH: Weinheim, 2005; ISBN 3527307192.

12. Heusch, R. Emulsions. In *Ullmann's Encyclopedia of Industrial Chemistry*; Wiley-VCH Verlag GmbH & Co. KGaA: Weinheim, Germany, 2000; Vol. 12, pp. 458–500.

13. Feinle, A.; Elsaesser, M.S.; Hüsing, N. Hierarchical Organization in Monolithic Sol–Gel Materials. In *Handbook of Sol-Gel Science and Technology*; Klein, L., Aparicio, A.J.M., Jitianu, A., Eds.; Springer, Cham: Switzerland, 2016; pp. 1–49.

14. Triantafillidis, C.; Elsaesser, M.S.; Hüsing, N. Chemical Phase Separation Strategies towards Silica Monoliths with Hierarchical Porosity. *Chemical Society Reviews* **2013**, *42*, 3833–3846, doi:10.1039/c3cs35345a.

15.   Everett, D.H. Manual of Symbols and Terminology for Physicochemical Quantities and Units, Appendix II: Definitions, Terminology and Symbols. *Colloid and Surface Chemistry* **1971**, *31*, 577–678, doi:10.1351/pac197231040577.

16.   Kosswig, K. Surfactants. In *Ullmann's Encyclopedia of Industrial Chemistry*; Wiley-VCH Verlag GmbH & Co. KGaA: Weinheim, Germany, 2000; Vol. 35, pp. 431–505.

17.   Hüsing, N. Porous Hybrid Materials. In *Hybrid Materials. Synthesis, Characterization, and Applications.*; Kickelbick, G., Ed.; Wiley - VCH: Weinheim, Germany, 2007; pp. 175–223 ISBN 9783527312993.

18.   Cardon, L.K.; Ragaert, K.J.; de Santis, R.; Gloria, A. Design and fabrication methods for biocomposites. In *Biomedical Composites*; Ambrosio, L., Ed.; Woodhead Publishing, 2017; pp. 17–36.

19.   Yadegari, A.; Fahimipour, F.; Rasoulianboroujeni, M.; Dashtimoghadarm, E.; Omidi, M.; Golzar, H.; Tahriri, M.; Tayebi, L. Specific considerations in scaffold design for oral tissue engineering. In *Biomaterials for Oral and Dental Tissue Engineering*; Tayebi, L., Moharamzadeh, K., Eds.; Woodhead Publishing Series in Biomaterials: Cambridge, United States, 2017; Vol. Part II, pp. 157–183 ISBN 9780081009673.

20.   Kaji, H.; Nakanishi, K.; Soga, N. Polymerization-Induced Phase Separation in Silica Sol-Gel Systems Containing Formamide. *Journal of Sol-Gel Science & Technology* **1993**, *1*, 35–46.

21.   Nakanishi, K. Pore Structure Control of Silica Gels Based on Phase Separation. *Journal of Porous Materials* **1997**, *4*, 67–112.

22.   *Handbook of Porous Solids*; Schiith, F., Sing, K.S.W., Weitkamp, J., Eds.; First Edition.; Wiley-VCH: Weinheim, Germany, 2002;

23.   Huo, Q. Synthetic Chemistry of the Inorganic Ordered Porous Materials. In *Modern Inorganic Synthetic Chemistry*; Xu, R., Pang, W., Huo, Q., Eds.; Elsevier: Amsterdam, 2011; pp. 339–373 ISBN 9780444535993.

24.   Suib, S.L. Porous Metals and Metal Oxides. In *Comprehensive Inorganic Chemistry II: From Elements to Applications*; Reedijk, J., Poeppelmeier, K., Eds.; Elsevier Ltd: Amsterdam, Netherlands, 2013; Vol. 5, pp. 151–168 ISBN 9780080965291.

25.   Brinker, J. Porous Inorganic Materials. *Current Opinion in Solid State & Materials Science* **1996**, *1*, 798–805.

26.   Hüsing, N.; Hartmann, S. Inorganic–Organic Hybrid Porous Materials. In *Hybrid Nanocomposites for Nanotechnology*; Merhari, L., Ed.; Springer Nature: Boston, MA, 2009; pp. 131–171.

27.   Meynen, V.; Cool, P.; Vansant, E.F. Synthesis of Siliceous Materials with Micro- and Mesoporosity. *Microporous and Mesoporous Materials* **2007**, *104*, 26–38, doi:10.1016/j.micromeso.2006.12.003.

28.   Barton, T.J.; Bull, L.M.; Klemperer, W.G.; Loy, D.A.; McEnaney, B.; Misono, M.; Monson, P.A.; Pez, G.; Schere, G.W.; Vartuli, J.C.; et al. Tailored Porous Materials. *Chemistry of Materials* **1999**, *11*, 2633–2656, doi:10.1021/cm9805929.

29.   Wu, L.; Li, Y.; Fu, Z.; Su, B.-L. Hierarchically Structured Porous Materials: Synthesis and Applications in Energy Storage. *National Science Review* **2020**, *7*, 1667–1701.

30.   Feinle, A.; Elsaesser, M.S.; Hüsing, N. Sol-Gel Synthesis of Monolithic Materials with Hierarchical Porosity. *Chemical Society Reviews* 2016, *45*, 3377–3399.

31.   Hüsing, N.; Schubert, U. Aerogels - Airy Materials: Chemistry, Structure, and Properties. *Angewandte Chemie - International Edition* **1998**, *37*, 22–45, doi:10.1002/(sici)1521-3773(19980202)37:1/2<22::aid-anie22>3.0.co;2-i.

32.   Sun, M.H.; Huang, S.Z.; Chen, L.H.; Li, Y.; Yang, X.Y.; Yuan, Z.Y.; Su, B.L. Applications of Hierarchically Structured Porous Materials from Energy Storage and Conversion, Catalysis, Photocatalysis, Adsorption, Separation, and Sensing to Biomedicine. *Chemical Society Reviews* **2016**, *45*, 3479–3563, doi:10.1039/c6cs00135a.

33.   *Hierarchically Structured Porous Materials: From Nanoscience to Catalysis, Separation, Optics, Energy, and Life Science*; Su, B.-L., Sanchez, C., Yang, X.-Y., Eds.; First Edition.; Wiley-VCH: Weinheim, Germany, 2012; ISBN 9780470577578.

34.   Guo, X.; Wang, R.; Yu, H.; Zhu, Y.; Nakanishi, K.; Kanamori, K.; Yang, H. Spontaneous Preparation of Hierarchically Porous Silica Monoliths with Uniform Spherical Mesopores Confined in a Well-Defined Macroporous Framework. *Dalton Transactions* **2015**, *44*, 13592–13601, doi:10.1039/c5dt01672j.

35.   Shi, Z.G.; Feng, Y.Q. Synthesis and Characterization of Hierarchically Porous Silica Microspheres with Penetrable Macropores and Tunable Mesopores. *Microporous and Mesoporous Materials* **2008**, *116*, 701–704, doi:10.1016/j.micromeso.2008.05.010.

36.   Hüsing, N. Design of inorganic and inorganic-organic hybrid materials by sol-gel processing-from nanostructures to hierarchical networks. In *Sol-Gel Methods for Materials Processing*; Innocenzi, P., Zub, Y.L., Kessler, V.G., Eds.; Springer, Dordrecht, 2008; pp. 91–104.

37.   Kajihara, K.; Kuwatani, S.; Maehana, R.; Kanamura, K. Macroscopic Phase Separation in a Tetraethoxysilane - Water Binary Sol-Gel System. *Bulletin of the Chemical Society of Japan* **2009**, *82*, 1470–1476, doi:10.1246/bcsj.82.1470.

38.   Nakanishi, K.; Soga, N. Phase Separation in Gelling Silica-Organic Polymer Solution: Systems Containing Poly[Sodium Styrenesulfonate). *Journal of the American Ceramic Society* **1991**, *74*, 2518–2548.

39.   Kickelbick, Guido. Introduction to Hybrid Materials. In *Hybrid Materials. Synthesis, Characterization, and Applications*; Kickelbick, G., Ed.; Wiley - VCH: Weinheim, Germany, 2007; pp. 1–48 ISBN 9783527312993.

40.   Lu, X.; Hasegawa, G.; Kanamori, K.; Nakanishi, K. Hierarchically Porous Monoliths Prepared via Sol–Gel Process Accompanied by Spinodal Decomposition. *Journal of Sol-Gel Science and Technology* **2020**, *95*, 530–550, doi:10.1007/s10971-020-05370-4.

41.   Young, N.P.; Balsara, N.P. Flory–Huggins Equation. In *Encyclopedia of Polymeric Nanomaterials*; Kobayashi, S., Müllen, K., Eds.; Springer Berlin Heidelberg, 2014; pp. 1–7.

42.   Nakanishi, K. Macroporous Morphology Control by Phase Separation. In *Handbook of Sol-Gel Science and Technology*; Klein, L., Aparicio, M., Jitianu, A., Eds.; Springer, Cham, 2016; pp. 1–32.

43.   Nakanishi, K.; Sato, Y.; Ruyat, Y.; Hirao, K. Supramolecular Templating of Mesopores in Phase-Separating Silica Sol-Gels Incorporated with Cationic Surfactant. *Journal of Sol-Gel Science and Technology* **2003**, *26*, 567–570.

44.   Hüsing, N.; Schubert, U. Porous Inorganic-Organic Hybrid Materials. In *Functional Hybrid Materials*; Gómez-Romero, P., Sanchez, C., Eds.; Wiley-VCH: Weinheim, Germany, 2004; pp. 86–121 ISBN 3527304843.

45.   Figueira, R.B.; Silva, C.J.R.; Pereira, E. v. Organic–Inorganic Hybrid Sol–Gel Coatings for Metal Corrosion Protection: A Review of Recent Progress. *Journal of Coatings Technology and Research* **2014**, *12*, 1–35, doi:10.1007/s11998-014-9595-6.

46.   Stöber, W.; Fink, A.; Bohn, E. Controlled Growth of Monodisperse Silica Spheres in the Micron Size Range. *Journal of Colloid and Interface Science* **1968**, *26*, 62–68.

47.   van Helden, A.K.; Jansen, J.W.; Vrij, A. Preparation and Characterization of Spherical Monodisperse Silica Dispersions in Nonaqueous Solvents. *Journal of Colloid and Interface Science* **1981**, *81*, 354–368.

48.   Bogush, G.H.; Tracy, M.A.; Zukoski Iv, C.F. PREPARATION OF MONODISPERSE SILICA PARTICLES: CONTROL OF SIZE AND MASS FRACTION. *Journal of Non-Crystalline Solids* **1988**, *104*, 95–106.

49.   Crotts, G.; Park, G. Preparation of Porous and Nonporous Biodegradable Polymeric Hollow Microspheres. *Journal of Controlled Release* **1995**, *35*, 91–105.

50.   Cai, Y.; Chen, Y.; Hong, X.; Liu, Z.; Yuan, W. Porous Microsphere and Its Applications. *International Journal of Nanomedicine* **2013**, *8*, 1111–1120, doi:10.2147/IJN.S41271.

51.   van Blaaderen, A.; Kentgens, A.P.M. Particle Morphology and Chemical Microstructure of Colloidal Silica Spheres Made from Alkoxysilanes. *Journal of Non-Crystalline Solids* **1992**, *149*, 161–178.

52.   Grün, M.; Büchel, G.; Kumar, D.; Schumacher, K.; Unger, K.K. Rational Design, Tailored Synthesis and Characterisation of Ordered Mesoporous Silicas in the Micron and Submicron Size Range. *Studies in Surface Science* **2000**, *128*, 155–165.

53.   Do, K.I.; And, K.; Kim, H.T. Formation of Silica Nanoparticles by Hydrolysis of TEOS Using a Mixed Semi-Batch/Batch Method. *Journal of Sol-Gel Science and Technology* **2002**, *25*, 183–189.

54.   Giesche, H. Synthesis of Monodispersed Silica Powders I. Particle Properties and Reaction Kinetics. *Journal of the European Ceramic Society* **1994**, *14*, 189–204.

55.   Büchel, G.; Unger, K.K.; Matsumoto, A.; Tsutsumi, K. *Advanced Materials*. Weinheim, Germany 1998, pp. 1036–1038.

56.   Matsoukas, T.; Gulari, E. Dynamics of Growth of Silica Particles from Ammonia-Catalyzed Hydrolysis of Tetra-Ethyl-Orthosilicate. *Journal of Colloid and Interface Science* **1988**, *124*, 252–261.

57.   Bogush, G.H.; Zukoski IV, C.F. Uniform Silica Particle Precipitation: An Aggregative Growth Model. *Journal of Colloid and Interface Science* **1991**, *142*, 19–34.

58.   Yang, L.M.; Wang, Y.J.; Sun, Y.W.; Luo, G.S.; Dai, Y.Y. Synthesis of Micrometer-Sized Hard Silica Spheres with Uniform Mesopore Size and Textural Pores. *Journal of Colloid and Interface Science* **2006**, *299*, 823–830, doi:10.1016/j.jcis.2006.02.043.

59.   C. T. Kresge; M. E. Leonowicz; W. J. Roth; J. C. Vartuli; J. S. Beck Ordered Mesoporous Molecular Sieves Synthesized by a Liquid-Crystal Template Mechanism. *Nature* **1992**, *359*, 710–712.

60.   Bagshaw, S.A.; Prouzet, E.; Pinnavaiat, T.J. Templating of Mesoporous Molecular Sieves by Nonionic Polyethylene Oxide Surfactants. *Science* **1995**, *269*, 1242–1244.

61.   Waldron, K.; Wu, Z.; Wu, W.D.; Liu, W.; Zhao, D.; Chen, X.D.; Selomulya, C. Formation of Uniform Large SBA-15 Microspheres via Spray Drying. *Journal of Materials Chemistry A* **2014**, *2*, 19500–19508, doi:10.1039/c4ta05002a.

62.   Zhu, H.; Liu, Y.; Chen, J.; Li, X.; Gao, L.; Chen, J. A One-Step Ultrasonic Spray Pyrolysis Approach to Large-Scale Synthesis of Silica Microspheres. *Silicon* **2020**, *12*, 1667–1672, doi:10.1007/s12633-019-00261-y.

63.   Yang, H.; Vovk, G.; Coombs, N.; Sokolov, I.; Ozin, G.A. Synthesis of Mesoporous Silica Spheres under Quiescent Aqueous Acidic Conditions. *Journal of Materials Chemistry* **1998**, *8*, 743–750, doi:10.1039/a705746f.

64.   De, G.J.; Soler-Illia, A.A.; Crepaldi, E.L.; Grosso, D.; Sanchez, C. Block Copolymer-Templated Mesoporous Oxides. *Current Opinion in Colloid and Interface Science* **2003**, *8*, 109–126, doi:10.1016/S1359-0294Ž03.00002-5.

65.   Xia, H.; Wan, G.; Zhao, J.; Liu, J.; Bai, Q. Preparation and Characterization of Monodisperse Large-Porous Silica Microspheres as the Matrix for Protein Separation. *Journal of Chromatography A* **2016**, *1471*, 138–144, doi:10.1016/j.chroma.2016.10.025.

66.   Zhang, S.; Li, G.L.; Cong, H.L.; Yu, B.; Gai, X.Y. Size Control of Monodisperse Silica Particles by Modified Stöber Method. *Integrated Ferroelectrics* **2017**, *178*, 52–57, doi:10.1080/10584587.2017.1323548.

67.   Barbé, C.; Bartlett, J.; Kong, L.; Finnie, K.; Lin, H.Q.; Larkin, M.; Calleja, S.; Bush, A.; Calleja, G. Silica Particles: A Novel Drug-Delivery System. *Advanced Materials* **2004**, *16*, 1959–1966, doi:10.1002/adma.200400771.

68.   Ghosh, S.K. Functional Coatings. In; Gosh, S.K., Ed.; Wiley-VCH, 2006; pp. 1–25.

69.   Schwuger, M.-J.; Stickdornt, K.; Schomacker, R. Microemulsions in Technical Processes. *Chemical Reviews* **1995**, *95*, 849–864.

70.   Finnie, K.S.; Bartlett, J.R.; Barbé, C.J.A.; Kong, L. Formation of Silica Nanoparticles in Microemulsions. *Langmuir* **2007**, *23*, 3017–3024, doi:10.1021/la0624283.

71.   Malato, S.; Fernández-Ibáñez, P.; Maldonado, M.I.; Oller, I. Solar Photocatalytic Processes: Water Decontamination and Disinfection. In *New and Future Developments in Catalysis: Solar Photocatalysis*; Elsevier Inc., 2013; pp. 371–393 ISBN 9780444538727.

72.   Spasiano, D.; Marotta, R.; Malato, S.; Fernandez-Ibañez, P.; di Somma, I. Solar Photocatalysis: Materials, Reactors, Some Commercial, and Pre-Industrialized Applications. A Comprehensive Approach. *Applied Catalysis B: Environmental* **2015**, *170–171*, 90–123, doi:10.1016/j.apcatb.2014.12.050.

73.   Ohtani, B. Principle of Photocatalysis and Design of Active Photocatalysts. In *New and Future Developments in Catalysis: Solar Photocatalysis*; Elsevier Inc., 2013; pp. 121–144 ISBN 9780444538727.

74.   Lucchini, M.A.; Lizundia, E.; Moser, S.; Niederberger, M.; Nyström, G. Titania-Cellulose Hybrid Monolith for In-Flow Purification of Water under Solar Illumination. *ACS Applied Materials and Interfaces* **2018**, *10*, 29599–29607, doi:10.1021/acsami.8b09735.

75.   Simonsen, M.E.; Soegaard, E.G. Photocatalytic degradation of chloroform usinf a new type of photo-reactor. In *Sol-Gel Methods for Processing*; Innocenzi, P., Zub, Y.L., Kessler, V.G., Eds.; Springer, Dondrecht, 2008; pp. 421–426.
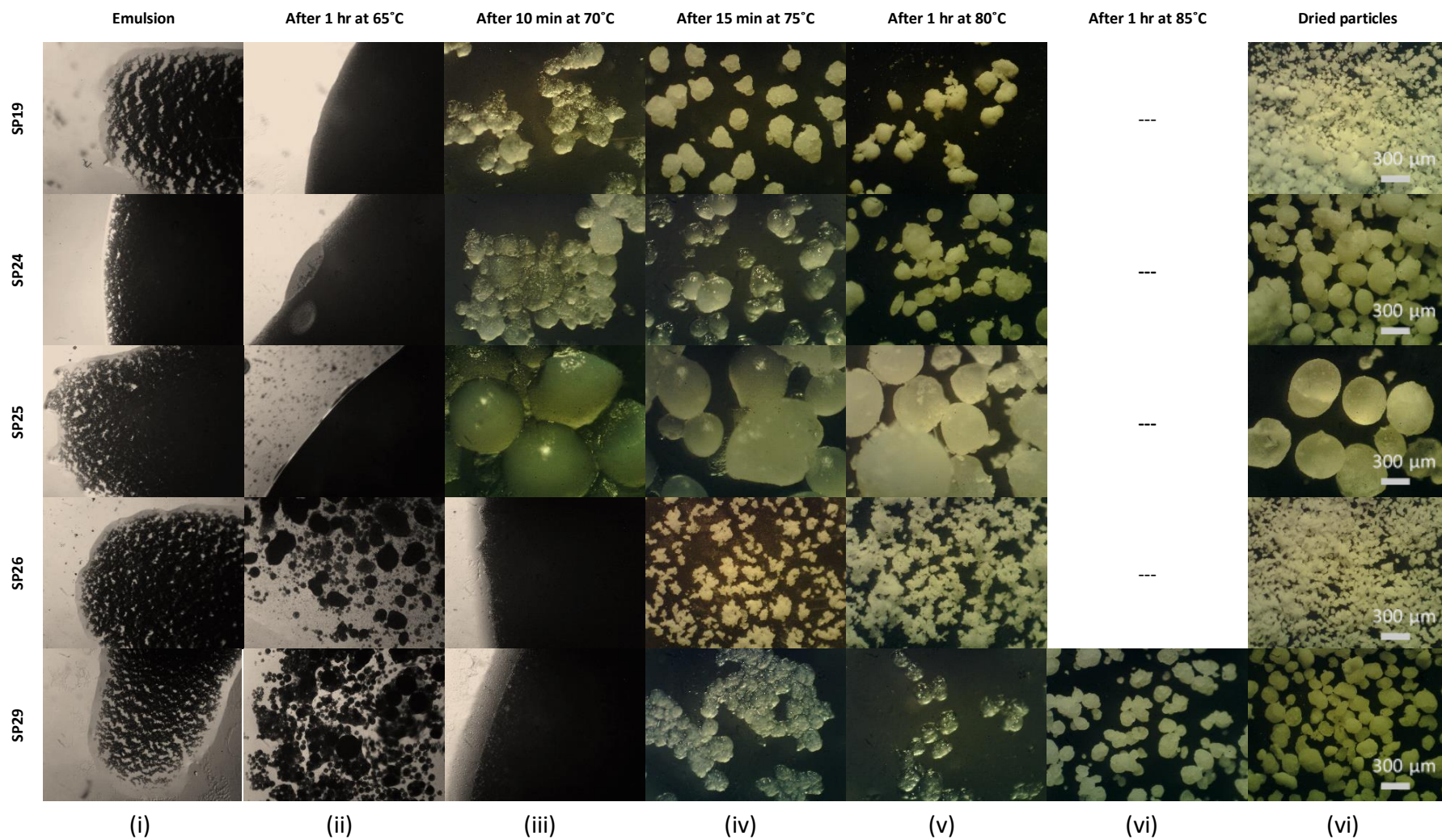
Appendix A

Figure 48 - Optical microscopy photographs of the reaction's medium according to the temperature and time described in Table 4 (i-vi). Bar scale = 300 μm.
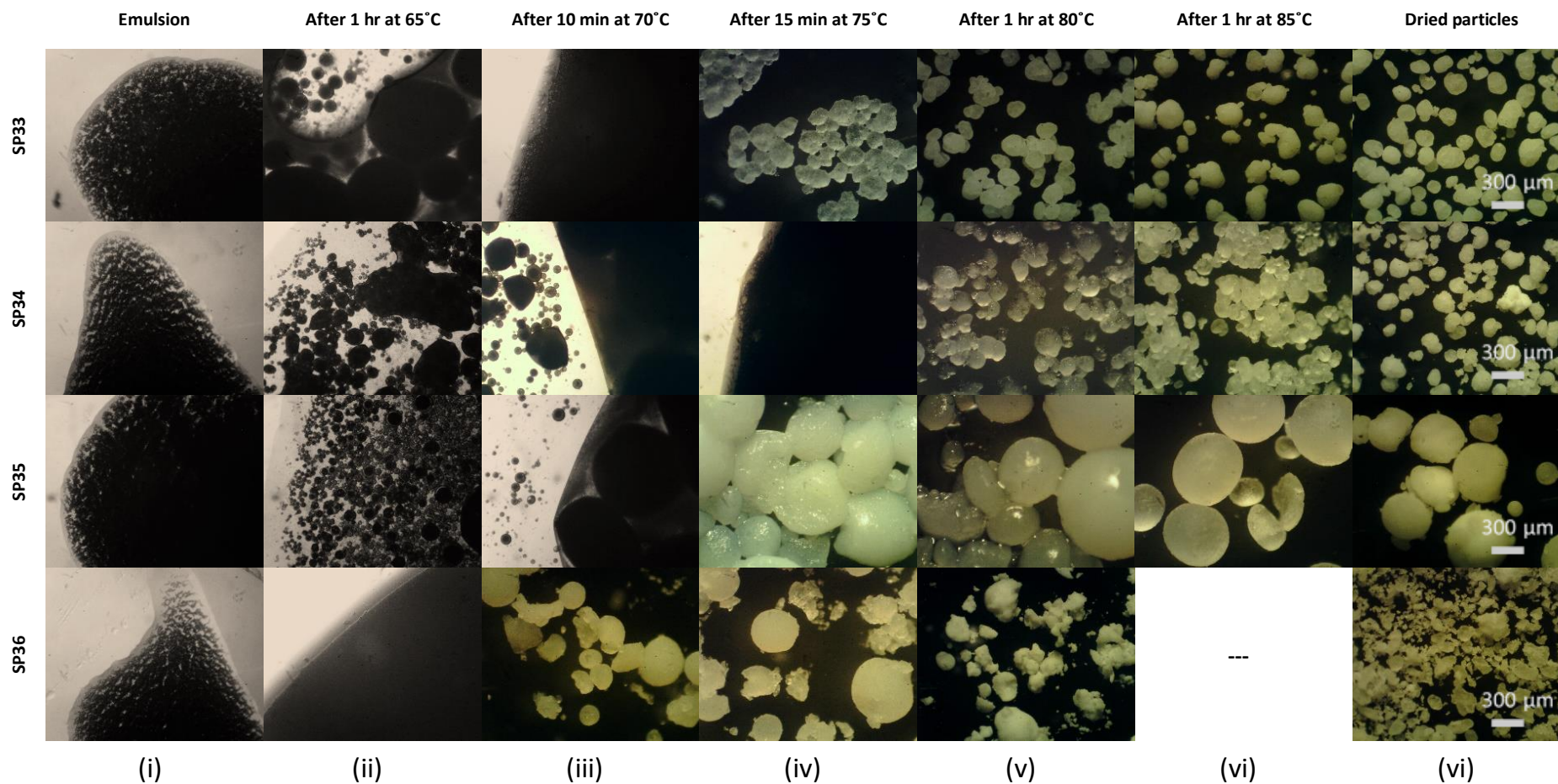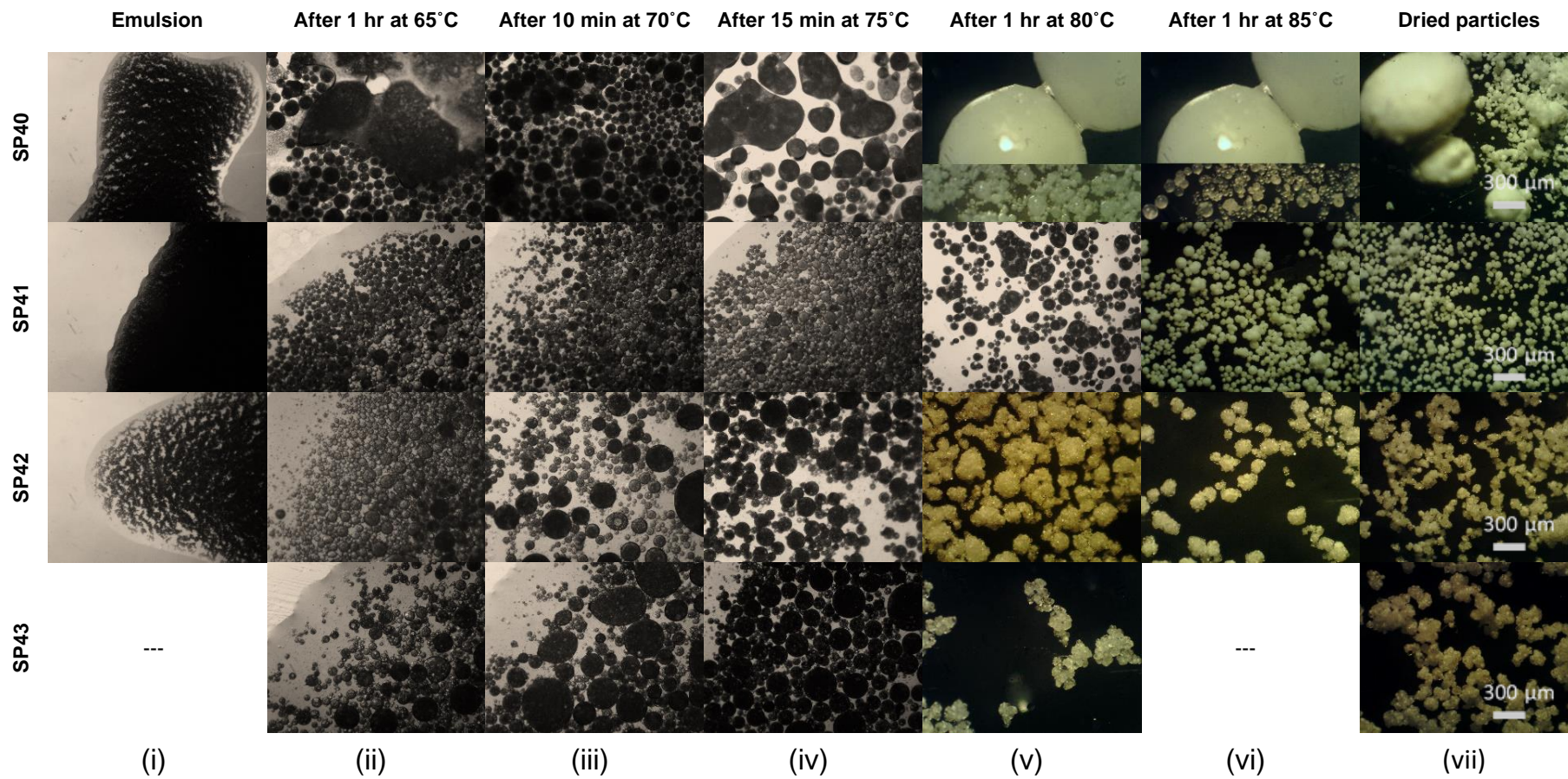
Appendix B

Figure 49 - Optical microscopy photographs of the reaction's medium according to the temperature and time described in Table 4 of the SP33-SP36 synthesis (i-vi). Bar scale = 300 μm.

Figure 50 - Optical microscopy photographs of the reaction's medium according to the temperature and time described in Table 4 of the SP40-SP43 synthesis (i-vii). Bar scale = 300 μm.
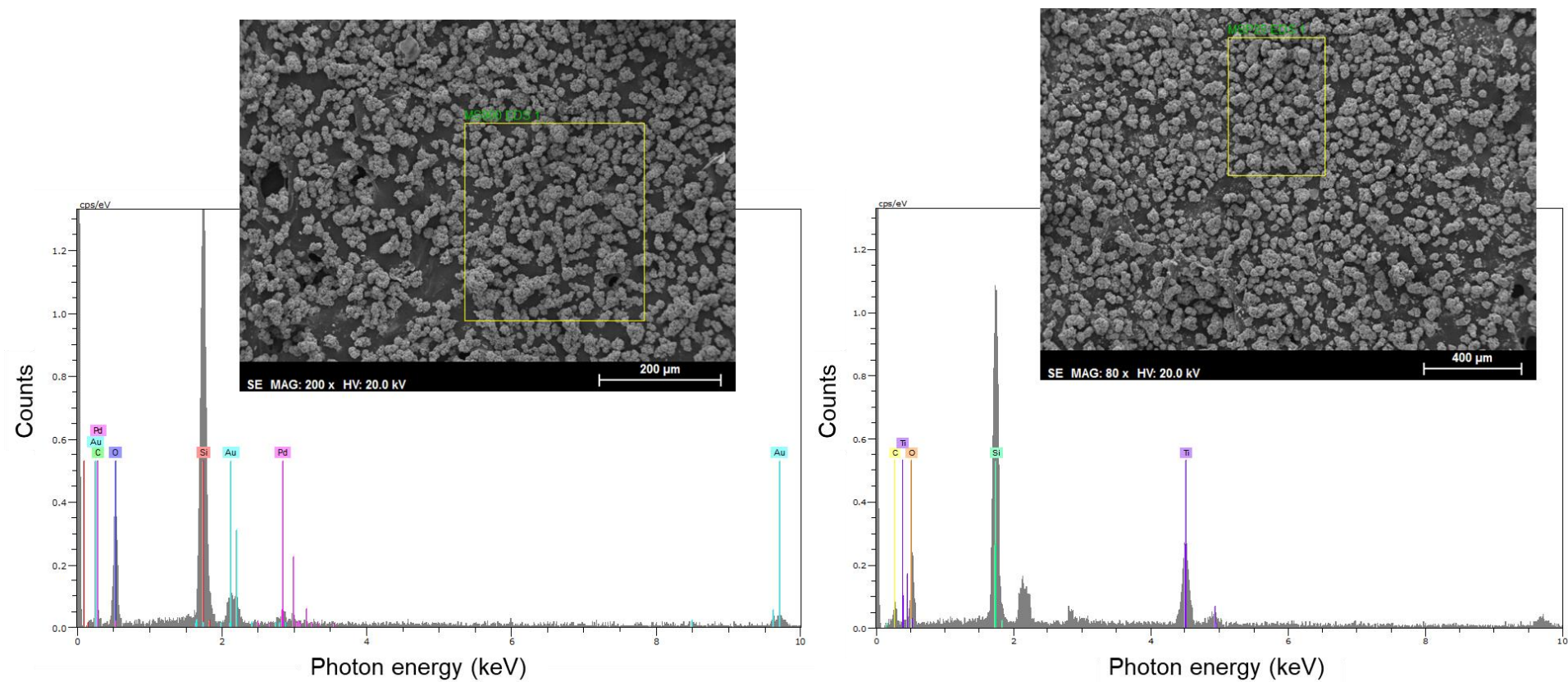
Appendix C

Figure 51 - EDX analysis for the SP26 MSs before (left) and after (right) the impregnation process.
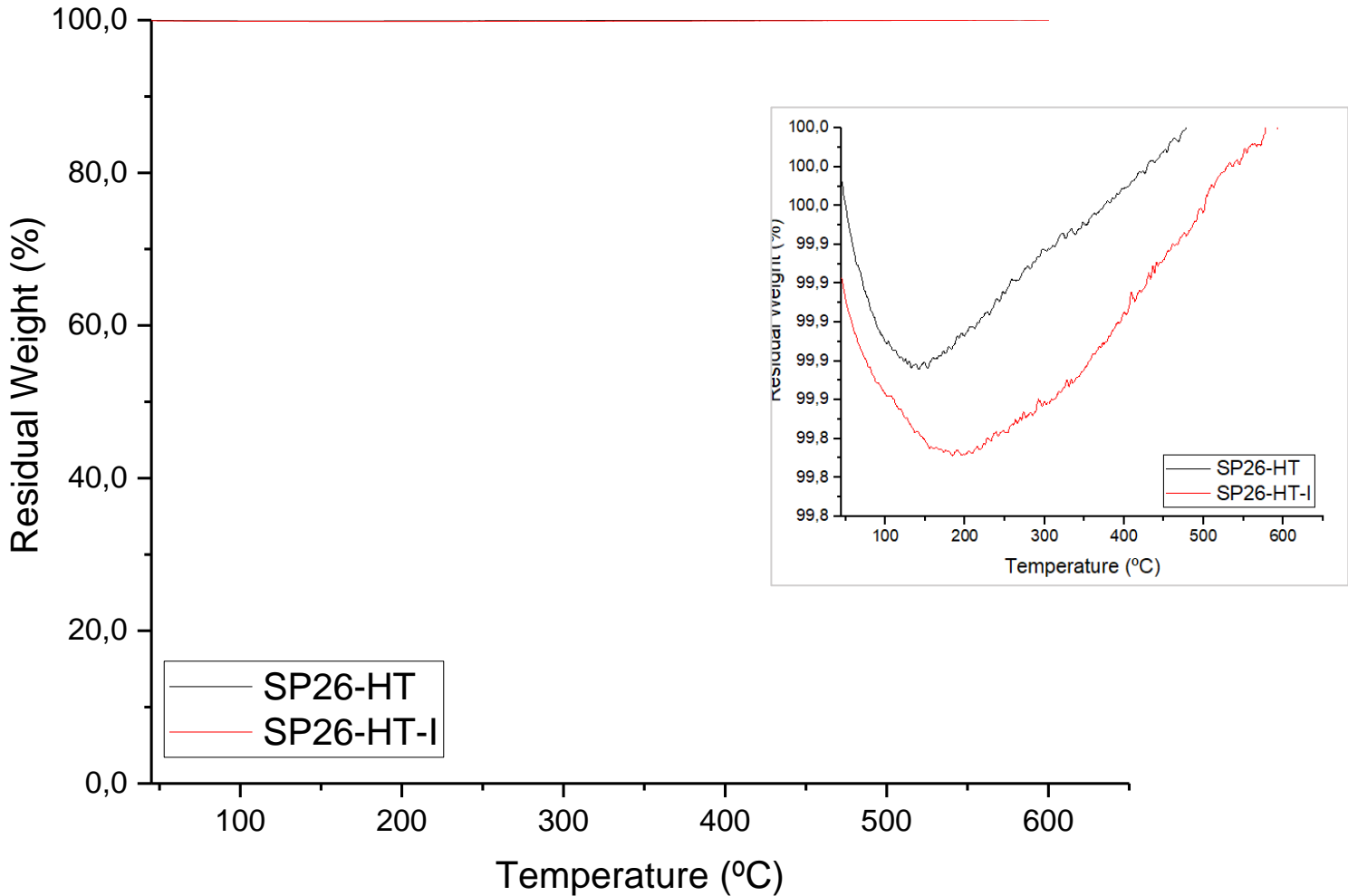
Appendix D

Figure 52 - TGA thermograms obtained for SP26 MSs before (black line) and after (red line) the impregnation process.